SPACE TELESCOPE SCIENCE INSTITUTE
Operated for NASA by AURA

Instrument Science Report WFC3 2004-004

Filter Ghosts in the WFC3 UVIS Channel

Thomas M. Brown & Olivia Lupie
April 14, 2004

ABSTRACT

We present the results of the first optical ghost testing on the WFC3 UVIS channel, performed as part of the mini-calibration that took place in December 2003 and January 2004. Overall, the optical performance of the UVIS channel is very good, with most of the 62 filters showing the expected low level of ghosting. However, a small subset of the filters show ghosting that is more problematic, due to the morphology and strength of the ghosts. We review the results of the mini-calibration ghost tests and describe the initial work to address the problem filters.

Introduction

The WFC3 UVIS channel was tested as part of a "mini-calibration" performed at NASA GSFC in December 2003 and January 2004. This was the first look at the UVIS channel performance, and WFC3 performed very well overall. See Reid (WFC3 ISR 2004-02) for a review of the entire test program.

WFC3 was designed as a general-purpose instrument that would complement the wide-field capabilities provided to HST by the ACS/WFC. The WFC3 UVIS CCD has greater sensitivity in the blue and near-UV than the ACS/WFC but lower sensitivity in the red - a direct consequence of optimizing the CCD at blue wavelengths. The WFC3 UVIS filters pushed the technological envelope to sculpt the shape of the bandpasses; an ideal filter has sharp transitions in throughput at the long and short wavelength cutoffs and low light leak outside of the nominal bandpass. Some of the filters use metallic coatings and multiple substrates to achieve the desired bandpass, but these innovations can increase the ghosting.

The mini-calibration program originally included tests on a subset of the filters (F225W, F606W, and F814W) to inspect the optical ghosts using a series of short (unsaturated) and long (saturated) exposures at various field points on and off the detector. After unusual ghosts were seen in F225W and F606W, this plan was expanded to include ghost testing in all of the UVIS filters, and to measure the ghost behavior as a function of wavelength in a subset of the filters.

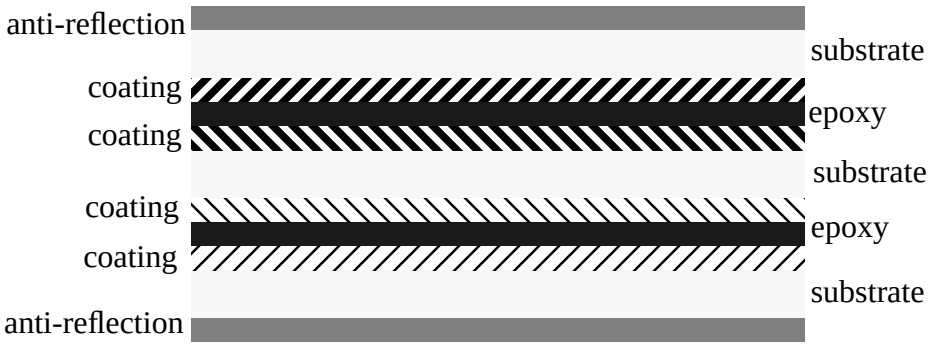

Figure 1 - The F606W filter consists of 3 substrates, 4 passband coatings, 2 anti-reflection coatings, and two epoxy layers, providing multiple surfaces for reflections and thus filter ghosts.

Figure 2 - A typical air gap filter (such as the F225W) consists of 2 substrates that are each coated on both sides, with an air gap in between. The selection of the substrate/coating combination depends upon the specific filter. Although the metallic coating provides good out-of-band blocking, it provides a reflective surface that can cause optical ghosts.

There are three classes of optical ghost in the WFC3 UVIS channel, due to

1. reflections between the CCD and the two windows
2. reflections between the window surfaces, and
3. reflections between the filter surfaces.

Stiavelli et al. (WFC3 ISR 2001-17) modelled the expected impact of ghosts due to reflections from a filter, 2 windows, and the CCD surface, but only considered a single-substrate filter. These models predicted the ghosting caused by reflections between the CCD and the windows, with faint donut-shaped ghosts well-separated from the primary image. However, because some of the filters are composed of multiple substrates (e.g., F606W, **Figure 1)**, while others are composed of multiple substrates with an air gap (e.g., F225W, **Figure 2**), the Stiavelli et al. (WFC ISR 2001-17) modeling did not predict the filter ghosts discovered during the mini-calibration. All three classes of ghost are present in the mini-calibration data, but the filter ghosts are the most problematic, with their unusual morphologies, strong intensities, and proximity to the primary image.

Procedure

The original test procedure employed a series of short and long exposures at various field points to measure the ghost behavior as a function of position for three filters: F225W, F606W, and F814W. There were 8 field points on the detector for each of the filters, and an additional series of field points for the F606W (12 on the detector and 16 immediately outside the field of view). Each short exposure is unsaturated, and provides a measure of the flux in the primary image. Each long exposure saturates the primary image, but provides an accurate measure of the flux in the ghosts. The strength of the ghosts can then be characterized as the ratio of the flux in the ghost to the flux in the primary image. The short exposures were taken as subarrays, while the long exposures were taken as full frames with 2x2 binned pixels. When strong and unusual ghosts were found in the original ghost tests, the testing was extended to include all of the filters, and to analyze the wavelength dependence of the ghosts in the F218W, F225W, and F606W filters. These later tests were usually done with short and long exposures both taken in an unbinned subarray, to reduce readout times, with the wavelength dependence measured at one field point and the position dependence measured at four field points.

The CASTLE optical stimulus at GSFC can provide a beam with varying size (simulating point-like and extended sources) and wavelength. Ghost tests were performed with the xenon lamp, which provides a very red spectrum (**Figure 3**) when the optical stimulus monochromators are not in use (i.e., for “white light” tests). The spectral energy distribution in the beam can be varied from nearly monochromatic (bandwidth from 1 to 13 nm,

using a double monochromator) to white light. When observing in white light, the spot size was 5 micron for filters at wavelengths shortward of 400 nm and 10 micron for filters at wavelengths longward of 400 nm, while the monochromatic tests were performed with a 200 micron spot. For reference, a 5 micron spot in the F218W filter typically had a FWHM of 2.5 pixels, while a 200 micron spot in the F218W filter produced a flat-topped profile of approximately 17 pixels in width (with shoulders extending several pixels beyond).

The analysis was done in IDL using the raw images (no pipeline processing). The primary image strength was measured using aperture photometry (10 pixel radius) with subtraction of local bias and background (30-50 pixel annulus). The ghost image strength was measured with subtraction of local bias and background, as determined by appropriate regions equally distant from the primary image. Ghosts were then characterized as a fraction of the net flux in the primary image.

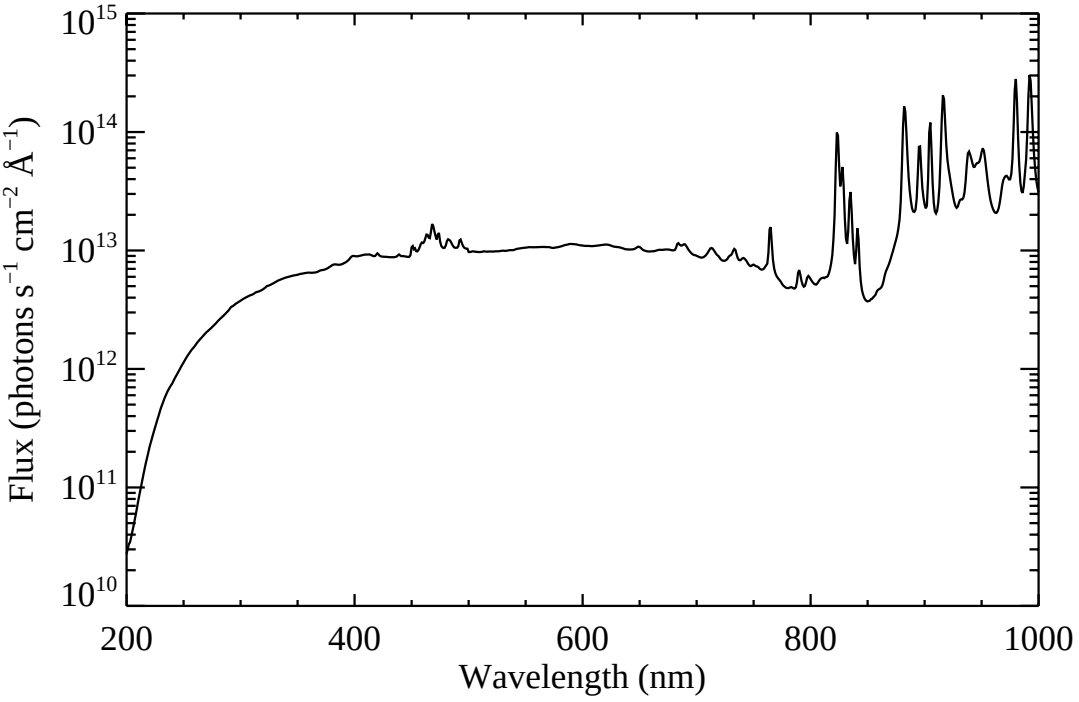

Figure 3: The spectrum of the xenon lamp provided by the CASTLE optical stimulus. Although the optical stimulus can provide both monochromatic and white light, the “white light” spectrum is actually very red.

Results

The results of the ghost testing are summarized in **Table 1**, and the filter images with significant ghosts are shown in **Figures 4 - 31**. Because the ghosts and data vary from filter to filter, there is no consistent metric for describing them. Multiple ghosts often overlap each other and features in the point spread function (e.g., diffraction spikes), so the estimates of the ghost strength relative to the primary image flux are approximate. Most of the filters showed ghosts that were well below the CEI specification of 0.2% per ghost. There are five categories where ghosts do not meet the specification:

1. When the primary image is placed in the lower right hand corner, ghosts appear along the detector diagonal at large distances from the primary image, and have a strength that is a few percent of that in the primary image (**Figure 4**). These are due to reflections between the CCD and window, and were predicted by the Stiavelli et al. (WFC3 ISR 2001-17) models. Full frame images with the target in this corner were only taken for a few filters, but these ghosts should appear in all filters.

2. At longer wavelengths, extended donut ghosts due to reflections between window surfaces appear near the primary image (~100 pixels; **Figures 4 & 21**) and can have strengths reaching several tenths of a percent of the primary image flux.

3. Some of the filters with metallic coatings also show strong ghosts due to reflections between the filter surfaces. These filter ghosts are extended and roughly donut-shaped, although the morphology varies strongly with field position. The position of the ghosts relative to the source also varies strongly with the position of the source on the detector. Examples are the air gap filters F218W (**Figure 5**) and F225W (**Figure 7**), and the single-substrate filer F280N (**Figure 24**). Monochromatic tests on the F218W (**Figure 6, Table 2**) and F225W (**Figure 8, Table 3**) filters show that the ghost strength is a strong function of wavelength.

4. Some of the multiple-substrate filters at long wavelengths show compact ghosts in addition to the extended window (donut) ghosts. These compact filter ghosts vary in size from point sources to resolved blobs several pixels across. The ghosts are most worrisome for the widely-used F606W (**Figures 14-16**). Curiously, the extended ghosts in F606W move dramatically with respect to the source as a function of source position (**Figure 14**), but the compact ghosts move very little (**Figure 15**). Monochromatic tests on the F606W (**Figure 16, Table 4**) show at least 13 compact ghosts, with the strength of each varying independently with wavelength.

5. Two of the filters show possible signs of surface degradation in addition to filter ghosts: F280N (**Figure 24**) and FQ243N (**Figure 23**). The F280N was checked at 8 field points (two distinct points in each quadrant). One field point in the upper right quadrant and one field point in the lower left quadrant each showed distinct unusual features. On the upper right, the source had a large halo in addition to the donut ghosts. On the lower left, large scattered light features radiated away from the source. The FQ243N filter was only checked at one field point (it is in a quad filter), but it also showed a large halo in addition to the donut ghosts.

Table 1: Results of Optical Ghosts for All UVIS Filters

Filter	Description	Summary of ghost properties
F218W	ISM feature	First filter ghost is ~8% of the primary image strength, total of filter ghosts is ~10% of the primary image strength, shapes and positions relative to primary image are unusual and field-dependent (**Figure 5**). Ghosts strengths are strongly wavelength-dependent (**Figure 6, Table 2**).
F225W	UV Wide	First filter ghost is ~10% of the primary image strength, total of filter ghosts is ~15% of the primary image strength, shapes and positions relative to primary image are unusual and field-dependent (**Figure 7**). Ghost strengths are strongly wavelength-dependent (**Figure 8, Table 3**).
F275W	UV Wide	Donut-shaped filter ghost with strength 0.7% of primary image, position relative to primary image is field-dependent (**Figure 9**)
F300X	Long Pass	Filter ghost is 1% of primary image, very unusual shape, shape and position relative to primary image are field-dependent (**Figure 10**)
F336W	U, Stromgren u	Ghosts < 0.1%
F350L	Long Pass	Ghosts < 0.1%
F390M	Long Pass	Ghosts < 0.1%
F390W	Washington C	Ghosts < 0.1%
F410M	Stromgren v	Unusual filter ghosts appearing as segmented donuts, brightest at 0.5%, next at 0.1%, shapes and positions of ghosts relative to primary image are field-dependent (**Figure 11**)
FQ422M	continuum	Ghosts < 0.1%
F438W	WFPC2 B	Ghosts < 0.1%
F467M	Stromgren b	Faint filter ghosts appearing as spots and donuts. Shapes and positions relative to primary image are field dependent, brightest at 0.2%, next at 0.1% (**Figure 12**).
F475W	SDSS g	Ghosts < 0.1%
F475X	Long Pass	Ghosts < 0.1%
F547M	Stromgren y	Faint filter ghosts appearing as spots and donuts. Shapes and positions of ghosts relative to primary image are field dependent, strength < 0.1% (**Figure 13**)
F555W	WFPC2 V	Ghosts < 0.1%
F600L	Long Pass	Ghosts < 0.1%
F606W	WFPC2 Wide V	Filter ghosts (spots) and window ghosts (donuts). Brightest spot is 0.1%, total flux in spots is 0.3%, total flux in donuts is 0.4%, donut positions relative to primary image are strongly field dependent (position angle and distance, **Figure 14**). The strengths of the spot ghosts are strongly wavelength dependent and distinct from each other (**Figure 15**, **Table 4**), and the position of the spot ghosts relative to the primary image only weakly depends upon source position on the detector (**Figure 16**).
F621M	11% passband	Filter ghosts (spots) and window ghosts (donuts). Brightest spot is 0.1%, total flux in spots is 0.3%, total flux in donuts is 0.4% (**Figure 17**). Similar field-dependent behavior to F606W, but spots vary more significantly with field position.

Table 1: Results of Optical Ghosts for All UVIS Filters

Filter	Description	Summary of ghost properties
F625W	SDSS r	Filter ghosts (spots) and window ghosts (donuts). Each ghost less than 0.1%, positions relative to primary image are field-dependent (**Figure 18**).
F689M	11% passband	Several window ghosts (donuts) totalling 0.5%, two filter ghosts (spots) at 0.1% each, positions of all relative to primary image are field-dependent (**Figure 19**).
F763M	11% passband	Ghosts < 0.1%
F775W	SDSS i	Filter ghosts (spots) and window ghosts (donuts). Each less than 0.1%, positions relative to primary are field-dependent (**Figure 20**).
F814W	WFPC2 Wide I	Three window ghosts (donuts): two interlocking donuts at 0.4%, one smaller donut at 0.1%. Positions relative to primary are field-dependent (**Figure 21**).
F845M	11% passband	Ghosts < 0.1%
F850L	SDSS z	Ghosts < 0.1%
FQ232N	CII] 2326	Two filter ghosts (donuts). Brightest 4%, next 1% (**Figure 22**).
FQ243N	[NeIV] 2425	Two filter ghosts (donuts). Brightest 2%, next 1% (**Figure 23**). Large halo around primary image, possibly due to surface degradation.
F280N	MgII 2795/2802	Some field points show overlapping filter ghosts (donuts; brightest 3%, total 10%) while other field points show signs of surface degradation (large halo around primary image at one position, and strong scattered light across the entire image at another position; **Figure 24**)
F343N	[NeV] 3426	Ghosts < 0.1%
F373N	[OII] 3726/3729	Ghosts < 0.1%
FQ378N	z ([OII] 3727)	Ghosts < 0.1%
FQ387N	[NeIII] 3869	Ghosts < 0.1%
F395N	CaII H&K	Ghosts < 0.1%
FQ436N	[OII] 4363 + Hg	Ghosts < 0.1%
FQ437N	[OIII] 4363	Ghosts < 0.1%
F469N	HeII 4686	Ghosts < 0.1%
F487N	H-b 4861	Ghosts < 0.1%
FQ492N	z (H-b)	Ghosts < 0.1%
F502N	[OIII] 5007	Ghosts < 0.1%
FQ508N	z ([OIII] 5007)	Ghosts < 0.1%
FQ575N	[NII] 5755	Ghosts < 0.1%
F588N	HeI 5876	Ghosts < 0.1%
FQ619N	CH4 6194	Ghosts < 0.1%
F631N	[OI] 6300	Ghosts < 0.1%
FQ634N	6194 continuum	Ghosts < 0.1%

Table 1: Results of Optical Ghosts for All UVIS Filters

Filter	Description	Summary of ghost properties
F645N	continuum	Ghosts < 0.1%
F656N	H-a 6563	Window ghosts (donuts) totaling 0.4% and filter ghosts (donuts) totaling 0.5% (**Figure 25**).
F657N	Wide Ha+[NIII]	Ghosts < 0.1%
F658N	[NII] 6583	Window ghosts (donuts) totaling 0.4% and a segmented filter ghost at 0.9% (**Figure 26**).
F665N	z (H-a + [NII])	Window ghosts (donuts) totaling 0.4% and a segmented filter ghost at 0.4% (**Figure 27**)
FQ672N	[SII] 6717	Ghosts < 0.1%
F673N	[SII] 6717, 6731	Window ghosts (donuts) totaling 0.4% and a segmented filter ghost at 0.3% (**Figure 28**)
FQ674N	[SII] 6731	Ghosts < 0.1%
F680N	z (H-a + [NII])	Window ghosts (donuts) totaling 0.4% and a segmented filter ghost at 0.3% (**Figure 29**)
FQ727N	?CH4 7270	Ghosts < 0.1%
FQ750N	7270 continuum	Ghosts < 0.1%
FQ889N	25/km-agt	Ghosts < 0.1%
FQ906N	2.5/km-agt	Ghosts < 0.1%
FQ924N	0.25/km-agt	Ghosts < 0.1%
FQ937N	0.025/km-agt	Ghosts < 0.1%
F953N	[SIII] 9532	Ghosts < 0.1%

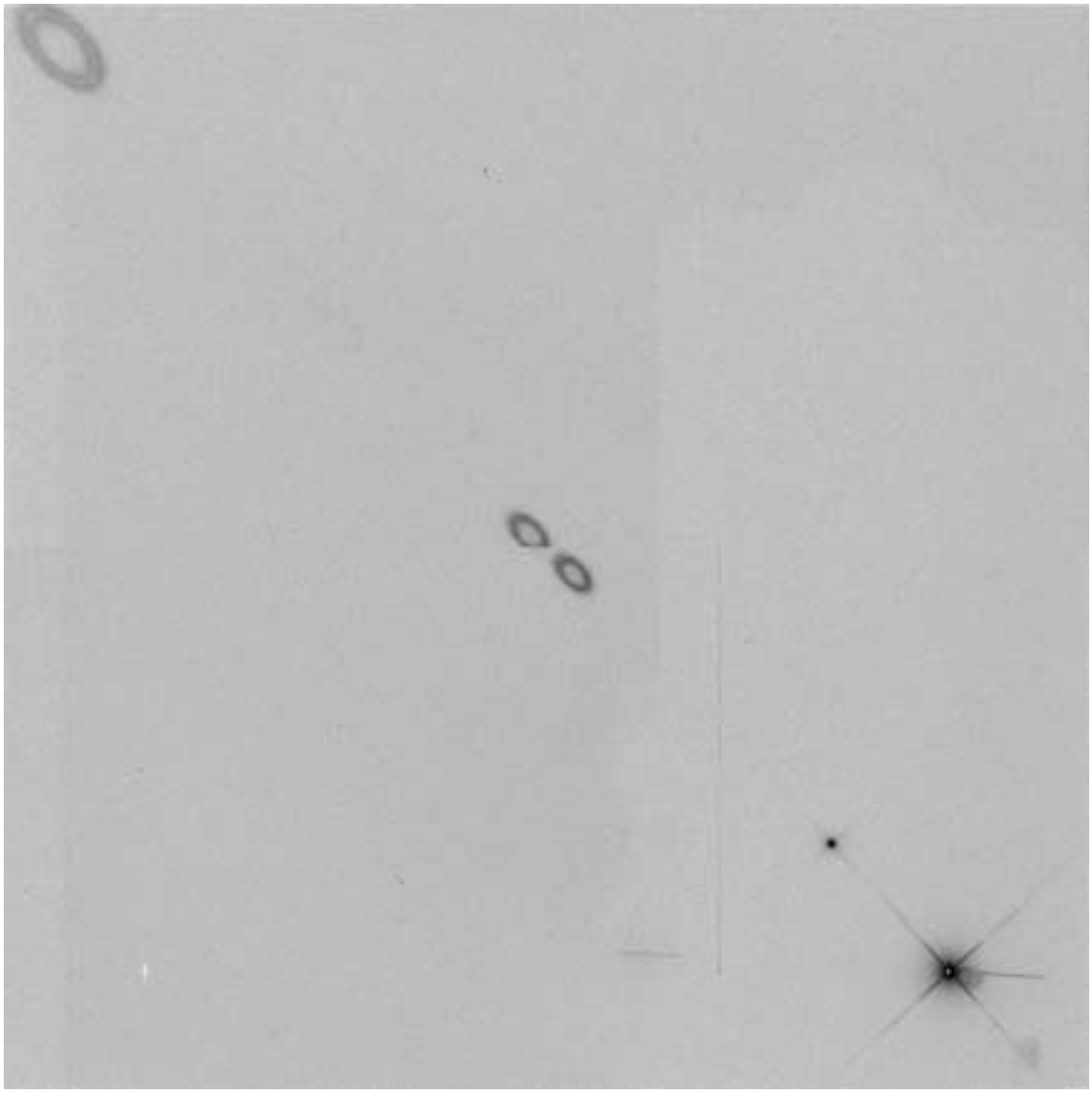

Figure 4 - An F814W full-frame image (saturated & log stretch) with the target in the lower right corner introduces ghosts well-separated from the primary image, as predicted by Stiavelli et al. (WFC3 ISR 2001-17), due to reflections between the CCD and windows. Smaller donut ghosts, due to reflections between the window surfaces, can be seen immediately to the right of the primary image. The irregular background, horizontal feature to the right of the primary image, and the extra point source are all artifacts of the test apparatus. One of the ghosts in the center is clipped by the gap between the two detector halves. The total flux in ghosts is approximately 3% of the source flux.

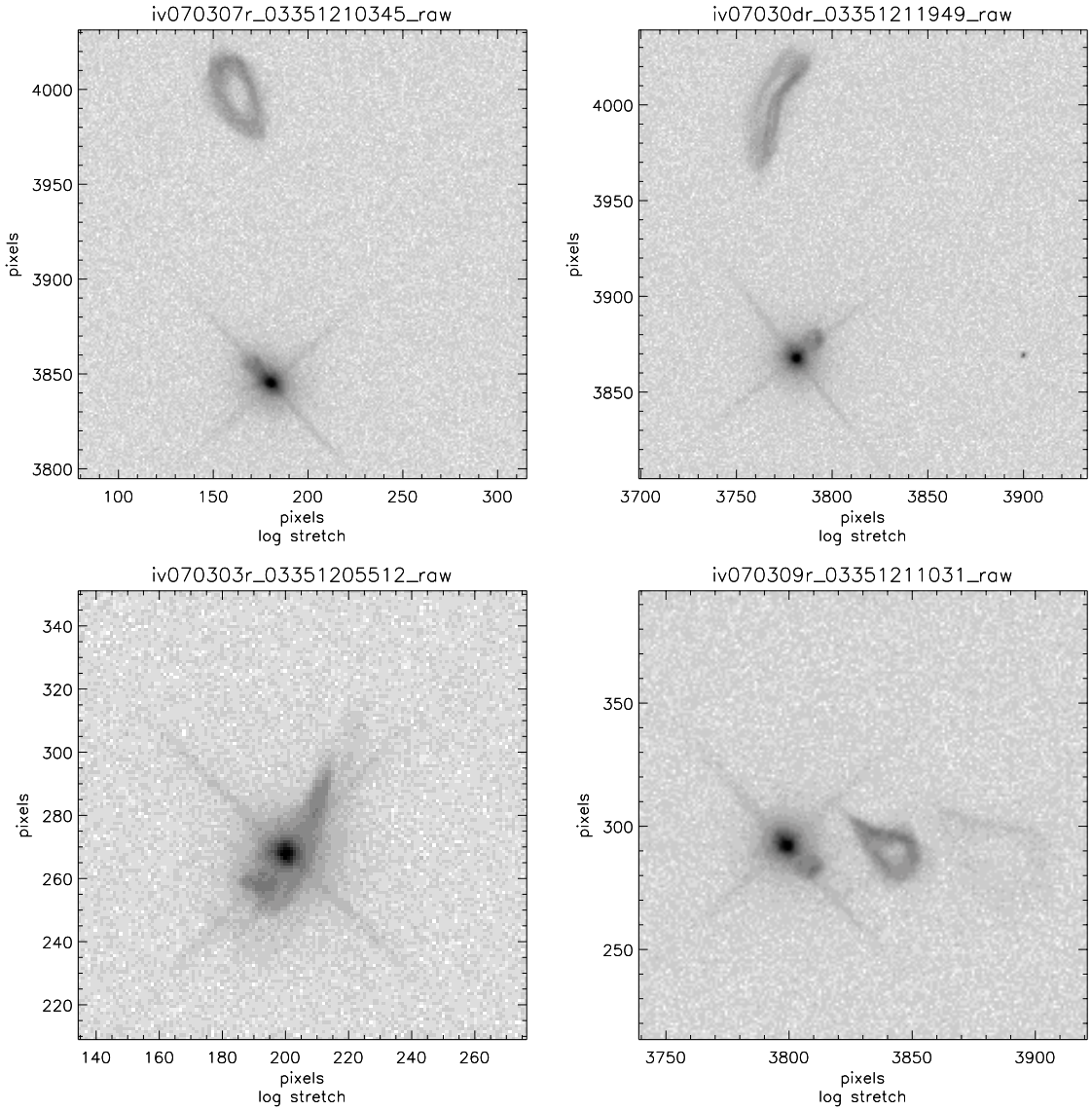

Figure 5 - F218W white light images (log stretch & saturated) with the source in each quadrant. This is an air gap filter. The title in each panel is the name of the FITS file from the test.The flux in the brightest filter ghost is about 8% of the source flux.

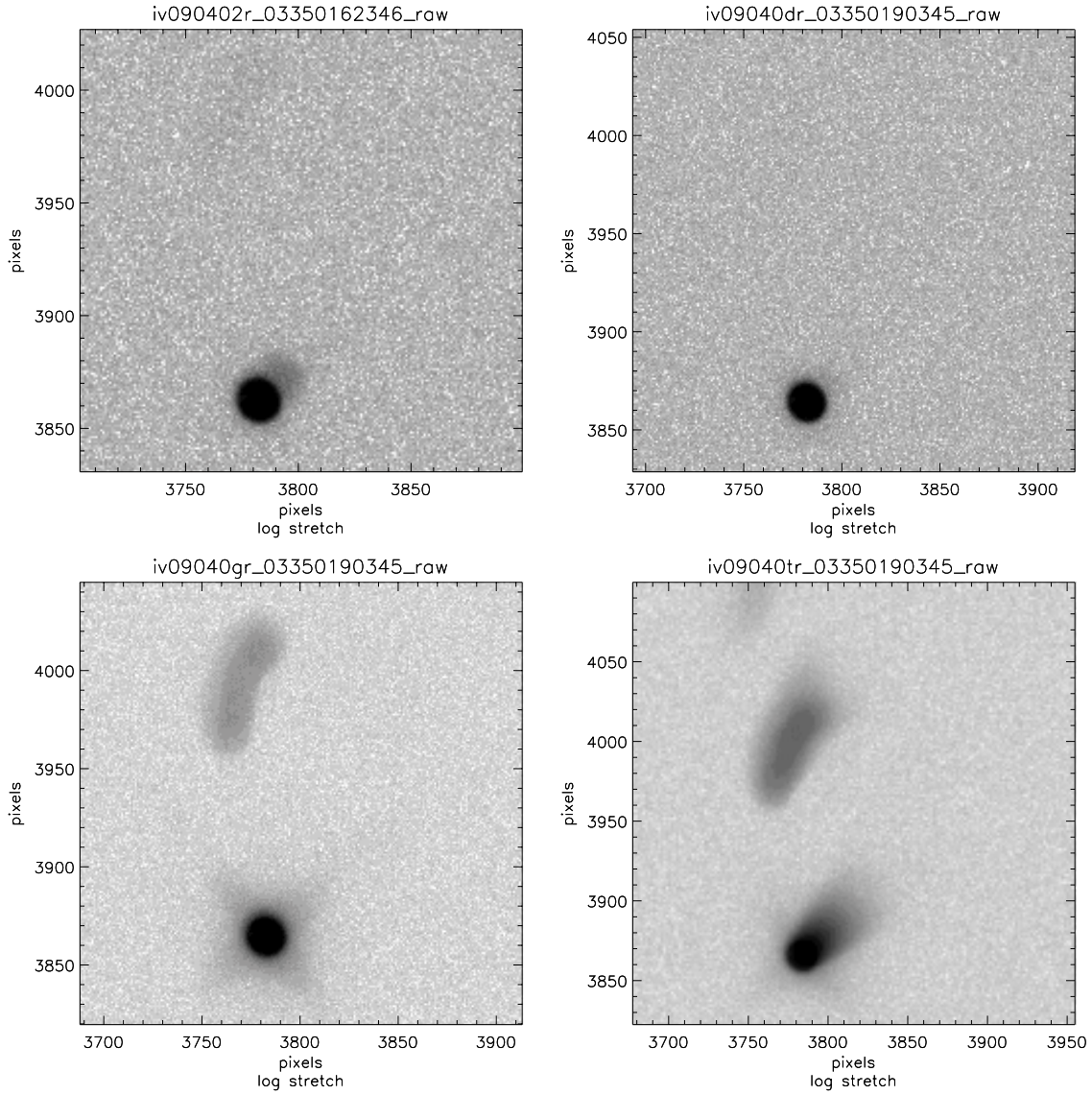

Figure 6 - F218W images (log stretch) of an extended monochromatic target, all at the same field point, for wavelengths of 200, 215, 240, and 270 nm. Most of the power in the ghosts comes from out of band light.

Table 2: F218W Ghost Strength vs. Wavelength*

wavelength (nm)	1st Ghost (% Primary)	wavelength (nm)	1st Ghost (% Primary)
200	1.4	425	3.9
204	1.7	450	5.3
210	1.5	475	5.2
215	0.9	500	4.1
245	2.8	525	4.4
250	5.0	550	3.8
255	11	575	4.1
260	19	600	3.0
265	24	625	3.9
270	19	650	3.1
275	16	675	4.7
300	14	700	5.1
325	17	800	5.1
350	12	900	4.0
375	5.0	1000	6.6
400	7.8		

*Strengths of the first ghost in monochromatic light agree fairly well with the strength of the first ghost seen in “white light” through the F218W filter. If one takes the weighted average of the monochromatic ghosts in this table, where the weighting function is the product of the WFC3 throughput and xenon lamp spectrum, one would predict a 7% ghost in white light imaging of the xenon lamp through the F218W filter, compared to the 8% actually measured.

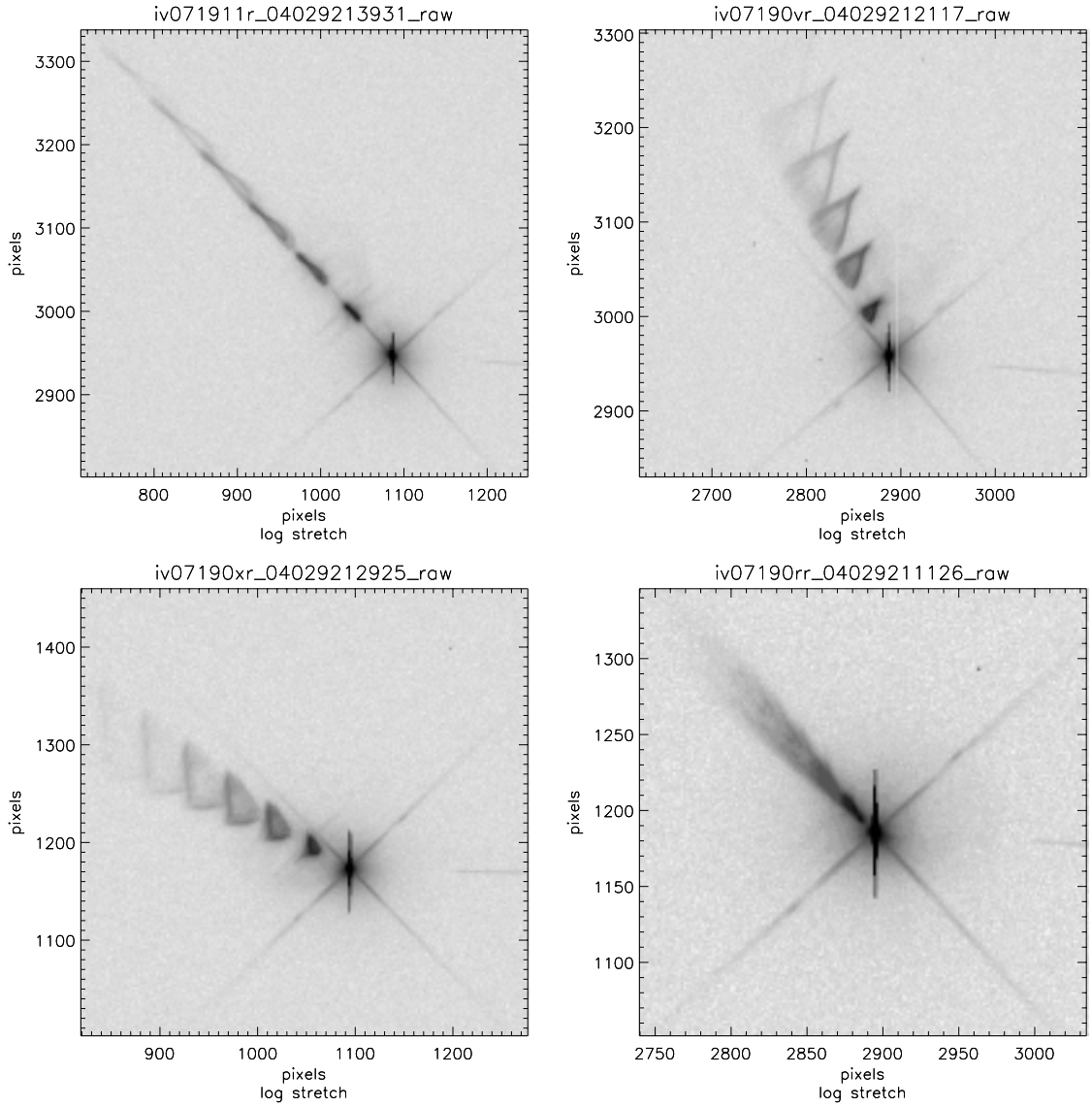

Figure 7 - F225W white light images (log stretch & saturated) with the source in each quadrant. This is an air gap filter. The horizontal feature to the right of the source is a test artifact. The flux in the brightest filter ghost is about 10% of the source flux. Note that we were only able to characterize ghosts that were more than a few pixels from the primary image. Besides the ghosts shown here, another family of filter ghosts falls almost on top of the primary image; these ghosts were impossible to see in most of the data, because they were obscured by the saturated core of the primary image, but were detectable as an asymmetry in the point spread function at a few field points.

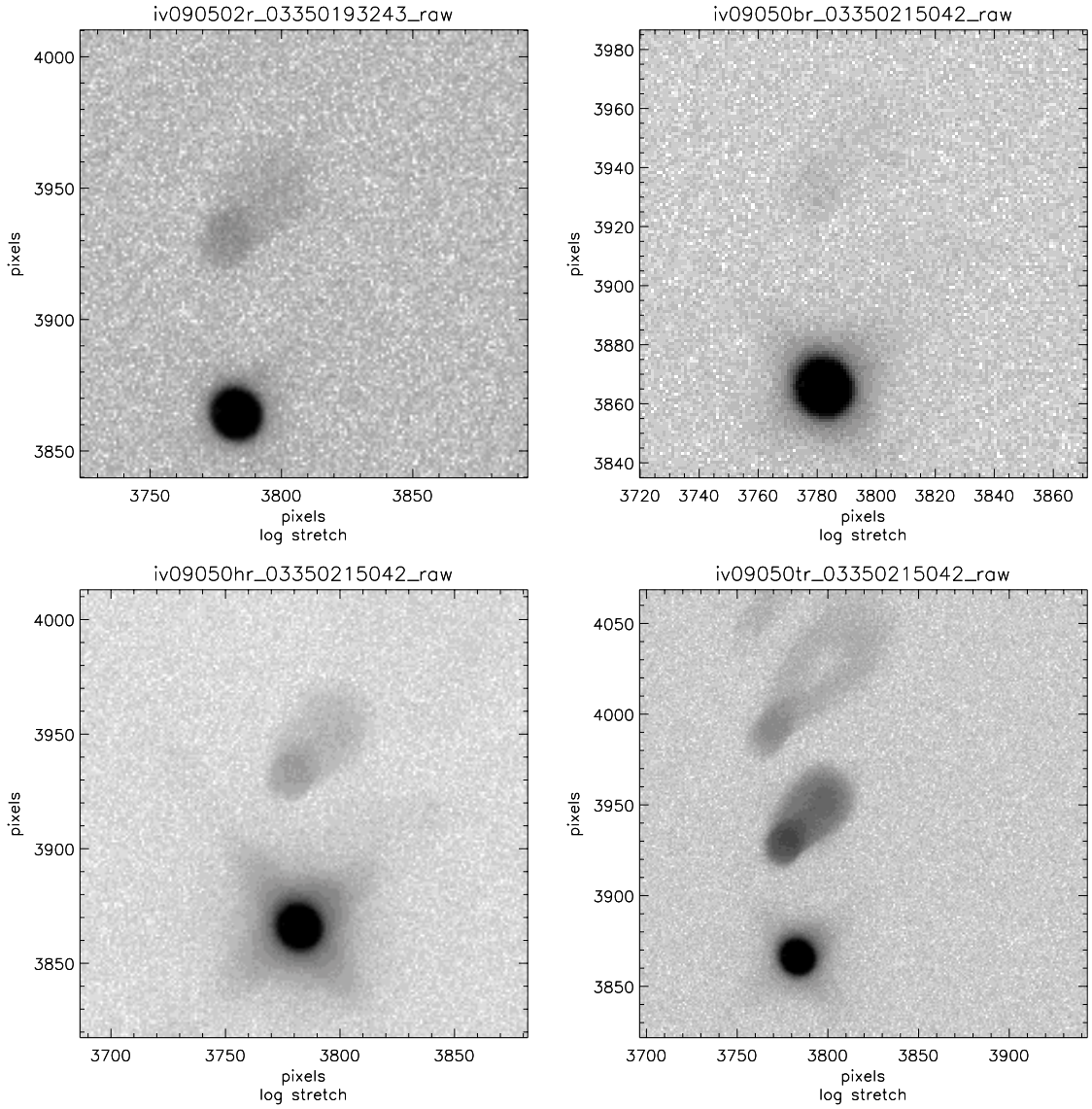

Figure 8 - F225W images (log stretch) of an extended monochromatic target, all at the same field point, for wavelengths of 200, 215, 240, and 270 nm. Most of the power in the ghosts comes from out of band light.

Table 3: F225W Ghost Strength vs. Wavelength*

wavelength (nm)	1st Ghost (% Primary)	wavelength (nm)	1st Ghost (% Primary)
200	4.6	375	2.2
204	2.8	400	14
210	1.4	425	2.6
215	0.4	450	9.4
220	0.2	475	4.5
230	0.2	500	5.3
240	0.5	525	6.0
245	0.4	550	3.6
250	1.1	575	3.6
255	4.6	600	4.3
260	10	625	4.1
265	16	650	4.0
270	23	675	3.1
275	28	700	3.0
300	34	800	2.4
325	35	900	5.4
350	18	1000	5.7

*Strengths of the first ghost in monochromatic light are not in perfect agreement with the strength of the first ghost seen in “white light” through the F225W filter. If one takes the weighted average of the monochromatic ghosts in this table, where the weighting function is the product of the WFC3 throughput and xenon lamp spectrum, one would predict a 7% ghost in white light imaging of the xenon lamp through the F225W filter, compared to the 10% actually measured. Also note that the “first” ghost reported here is the first ghost well-separated from the point spread function; there is another family of ghosts falling right on top of the primary image that can be detected as an asymmetry in the point spread function at a few field points, but these ghosts cannot be characterized due to the saturated primary image core.

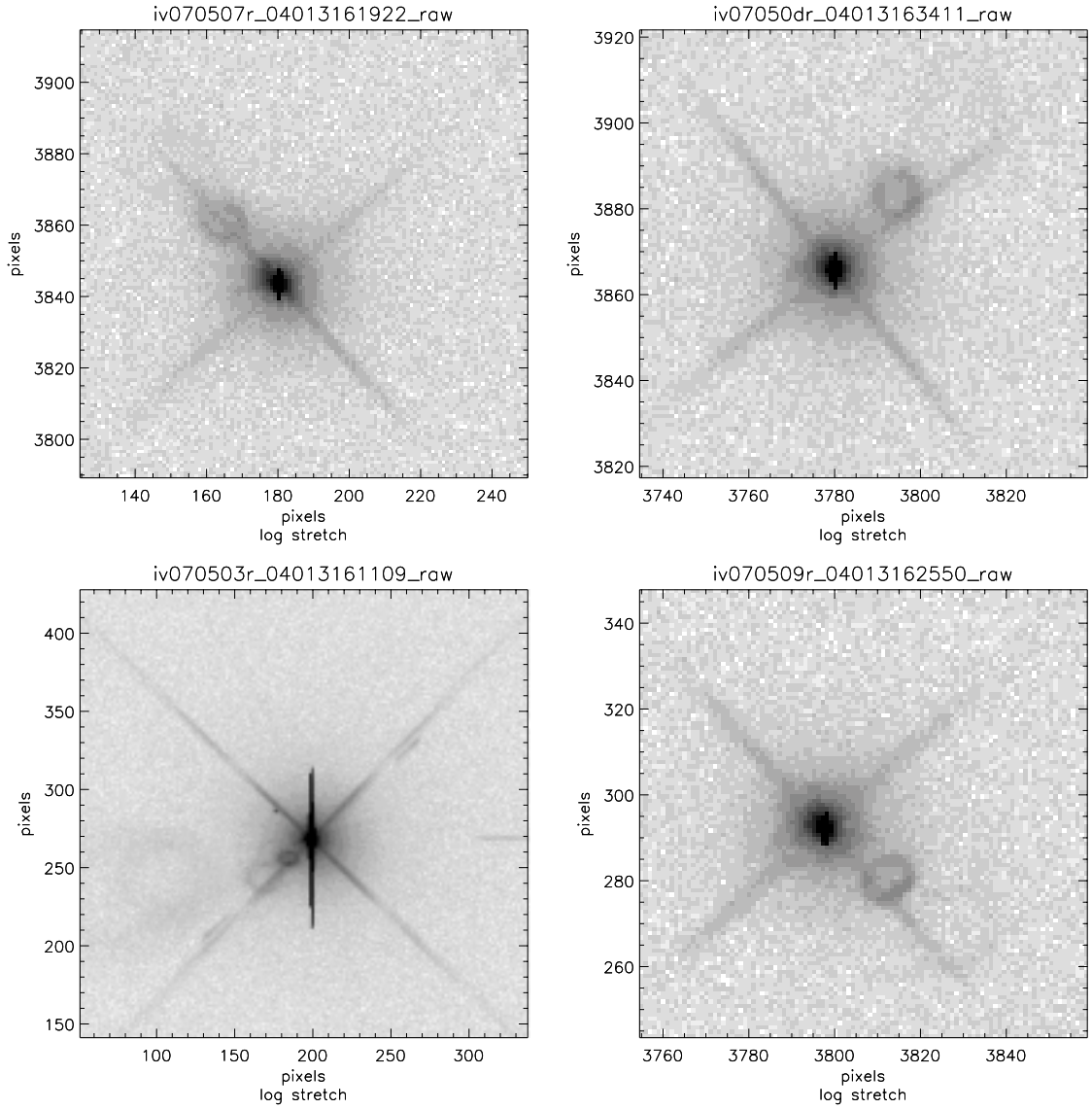

Figure 9 - F275W white light images (log stretch & saturated) with the source in each quadrant. On the lower left, the window ghosts appear as donuts that are more extended and fainter than the filter ghost. The horizontal feature to the right of the primary image is a test artifact. The flux in the brightest filter ghost is about 0.7% of the source flux.

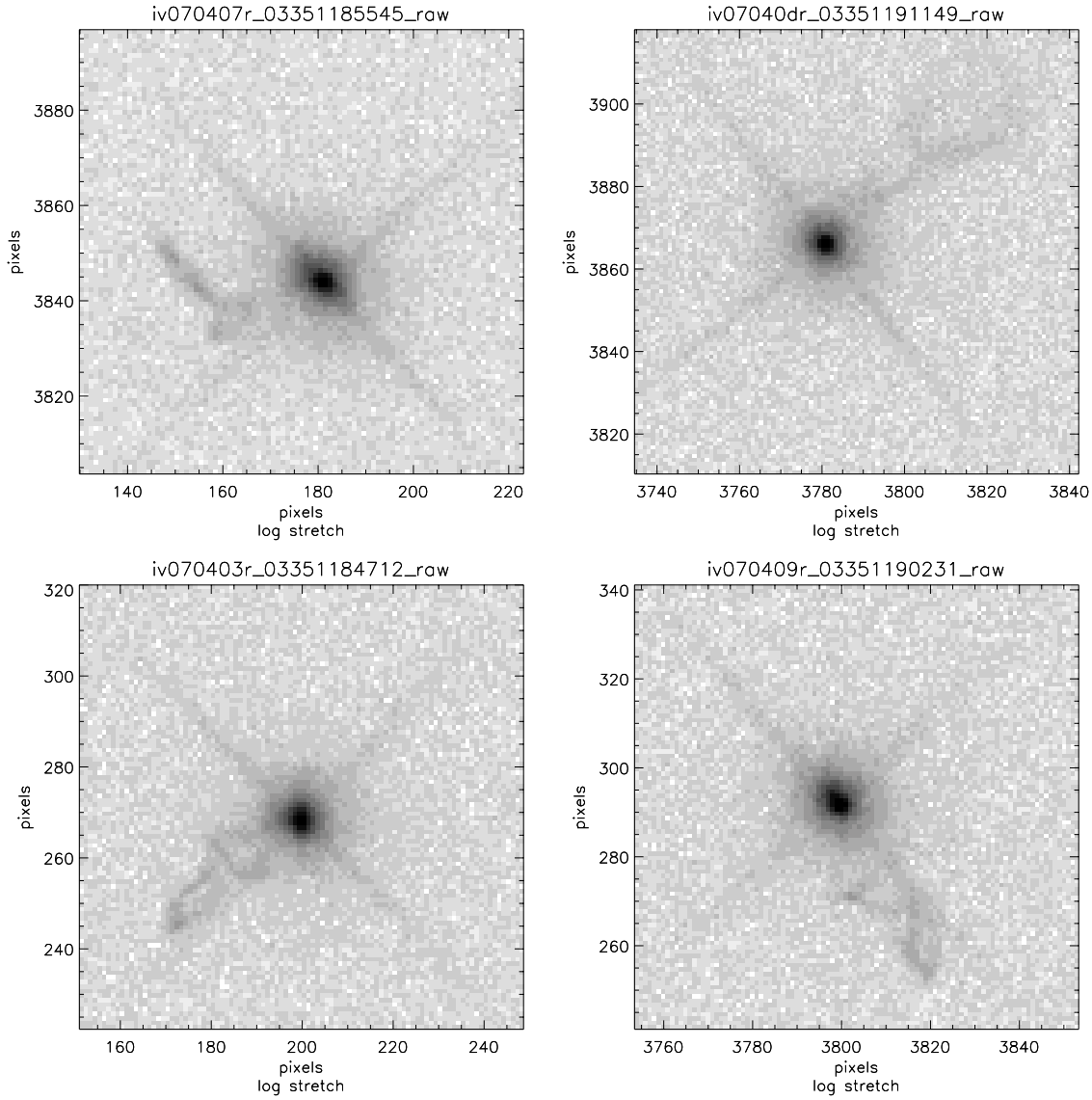

Figure 10 - F300X white light images (log stretch & saturated) with the source in each quadrant. This is an air gap filter. Although the filter ghost is only 1% the strength of the primary image, its unusual field-dependent morphology would be difficult to calibrate.

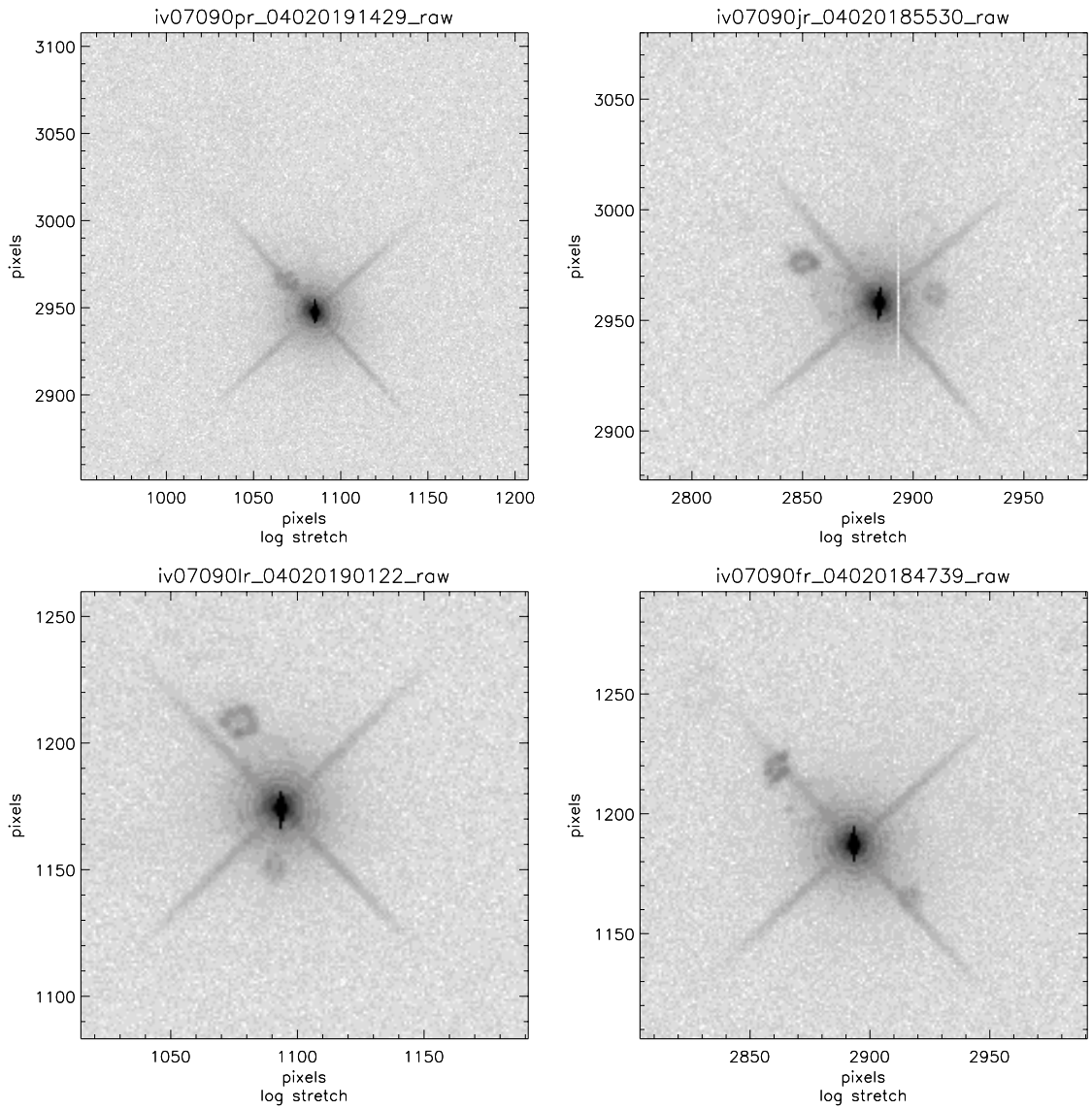

Figure 11 - F410M white light images (log stretch & saturated) with the source in each quadrant. The vertical feature in the upper right quadrant is a dead detector column. The flux in the brightest filter ghost is about 0.5% of the source flux.

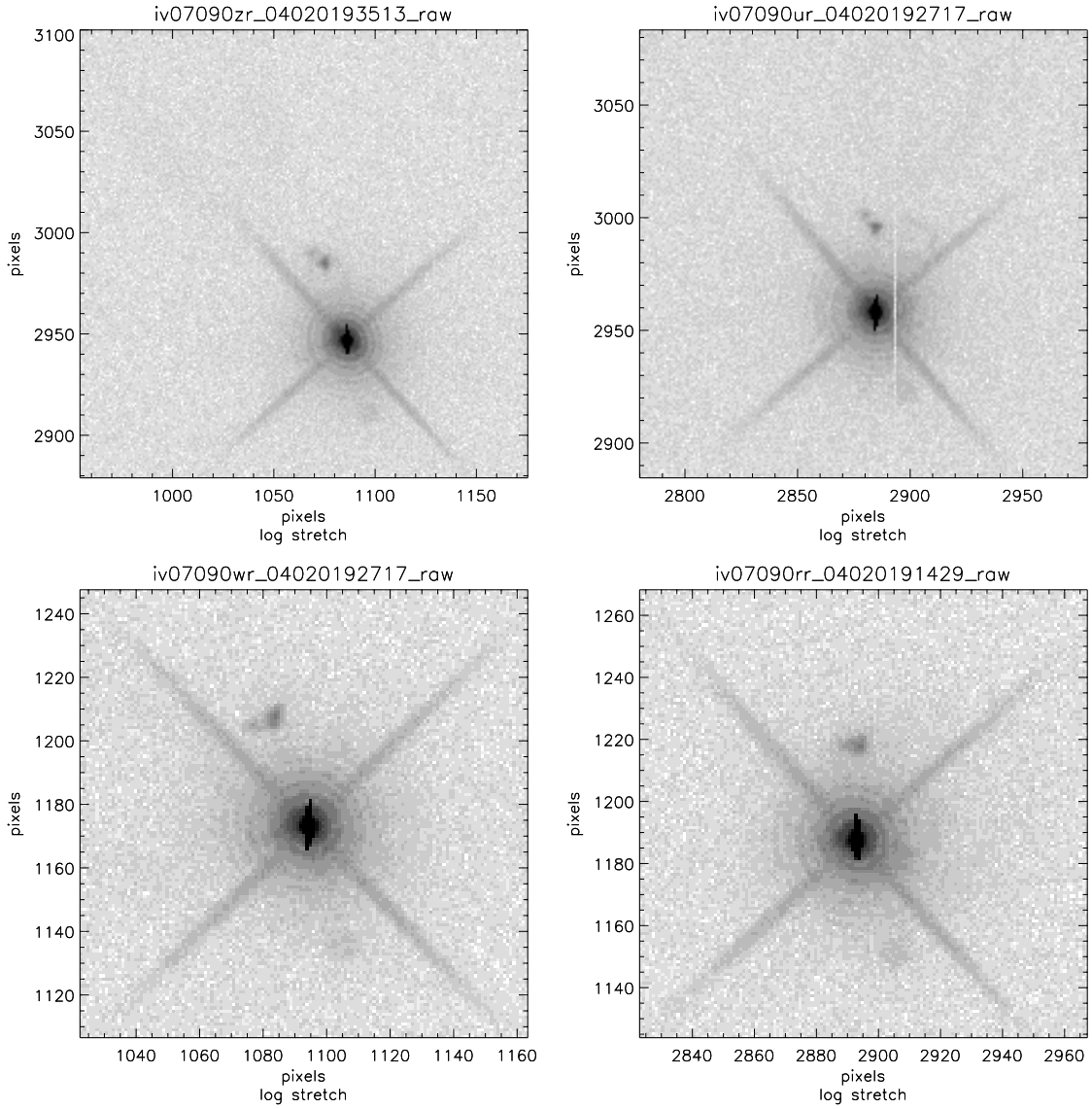

Figure 12 - F467M white light images (log stretch & saturated) with the source in each quadrant. The vertical feature in the upper right quadrant is a dead detector column. The flux in the brightest filter ghost is about 0.2% of the source flux.

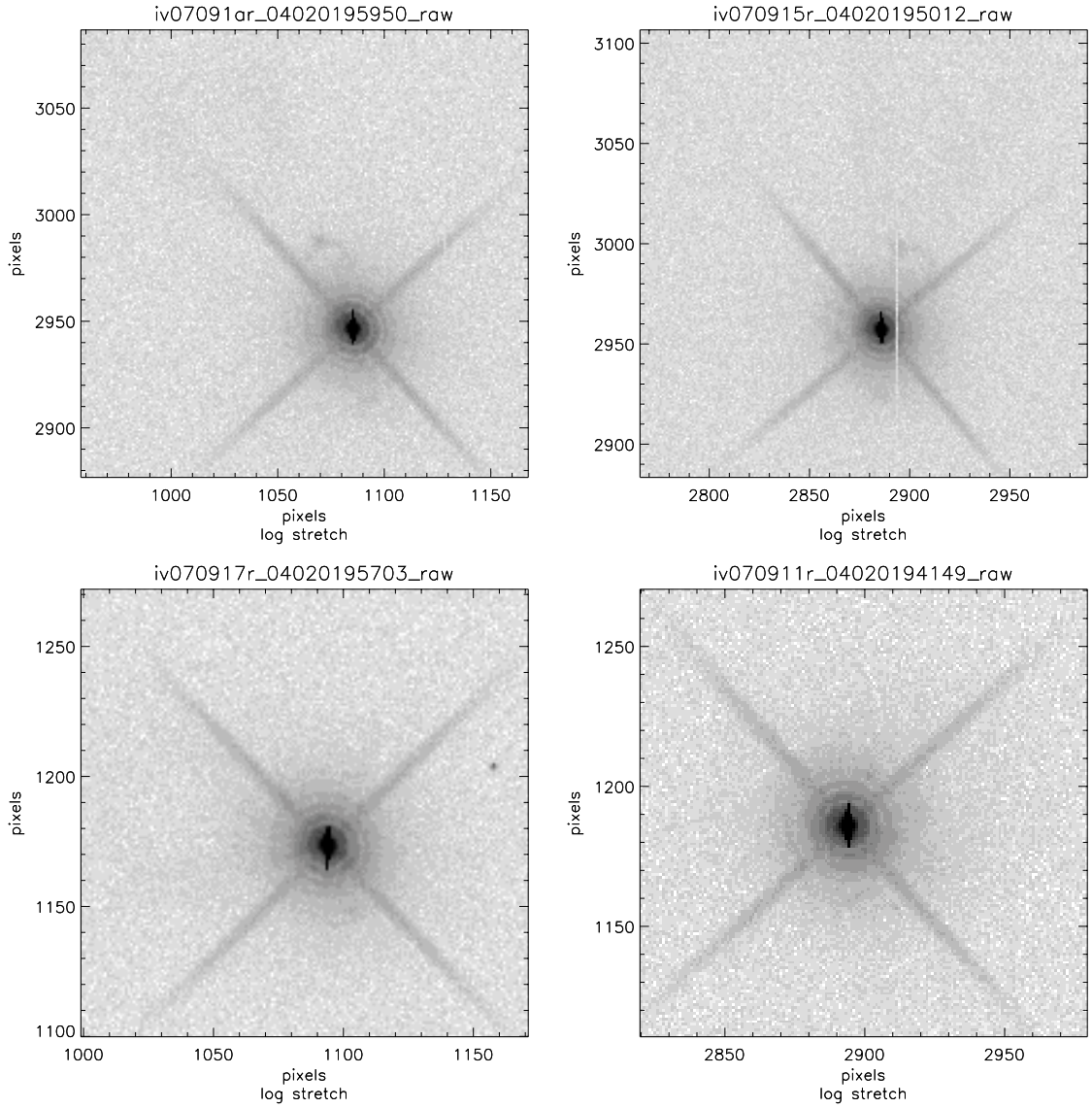

Figure 13 - F547M white light images (log stretch & saturated) with the source in each quadrant. The vertical feature in the upper right quadrant is a dead detector column. Extremely faint donuts from the window are present, along with a few compact ghosts from the filter. The flux in the brightest compact ghost is about 0.03% of the source flux.

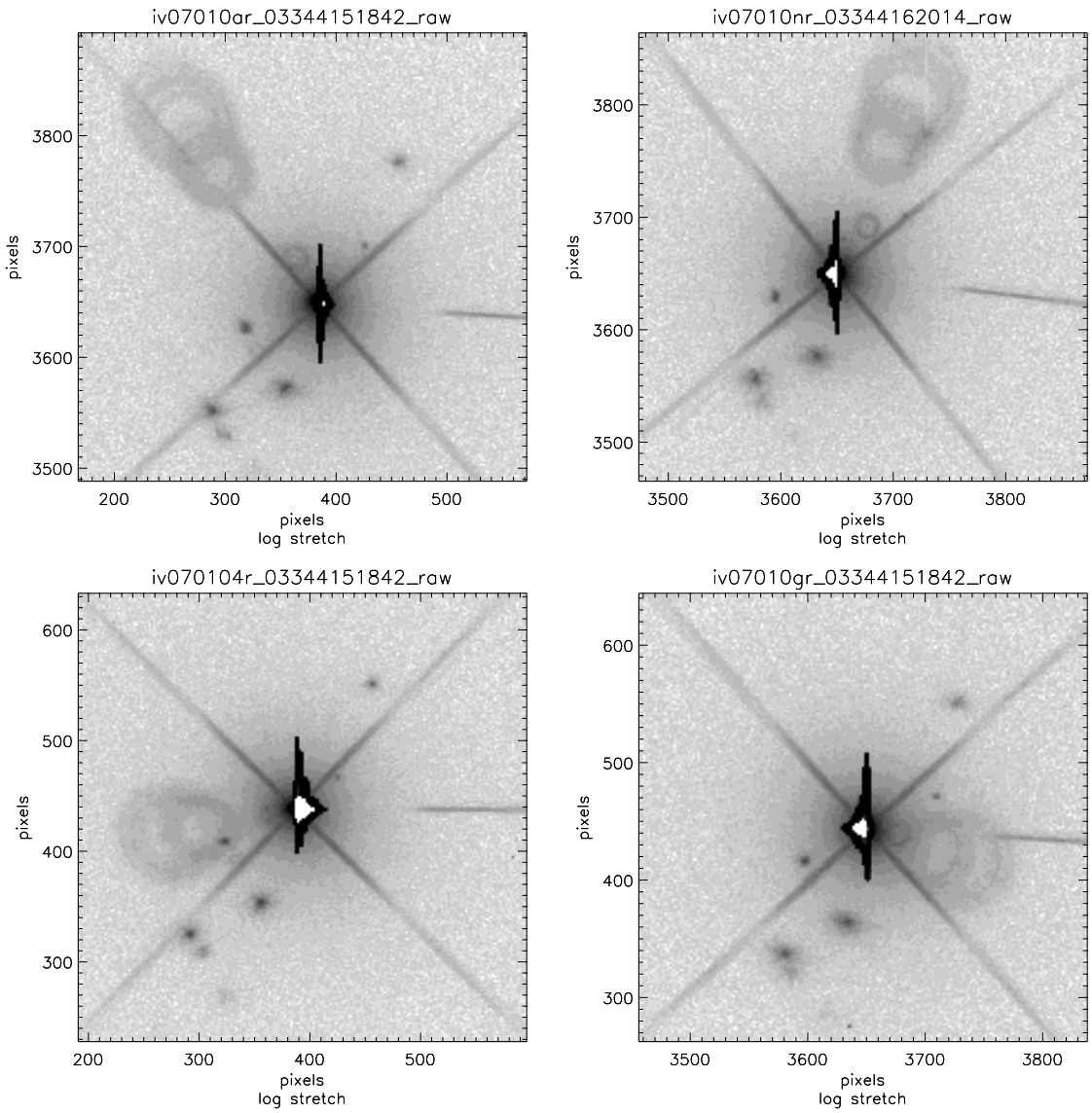

Figure 14 - F606W white light images (log stretch & saturated) with the source in each quadrant. These images were binned 2x2, but the scale has been adjusted to reflect positions in unbinned pixels (note that this correction has been performed on any data shown in this report that was taken with binning). The large extended donuts are window ghosts, while the smaller spots are filter ghosts. The flux in the two large overlapping donuts is about 0.3% of the source flux, while the flux in the smaller donut (near the source) is about 0.1% of the source flux. The flux in the brightest spot ghost is about 0.1% of the source flux. The strengths of the spot ghosts (13 detected in all) are a strong function of wavelength (see **Figure 15**). The window ghosts move significantly with respect to the primary image as a function of position on the detector, but the spot ghosts only move by a few pixels (see **Figure 16**). The horizontal feature to the right of the source is a test artifact.

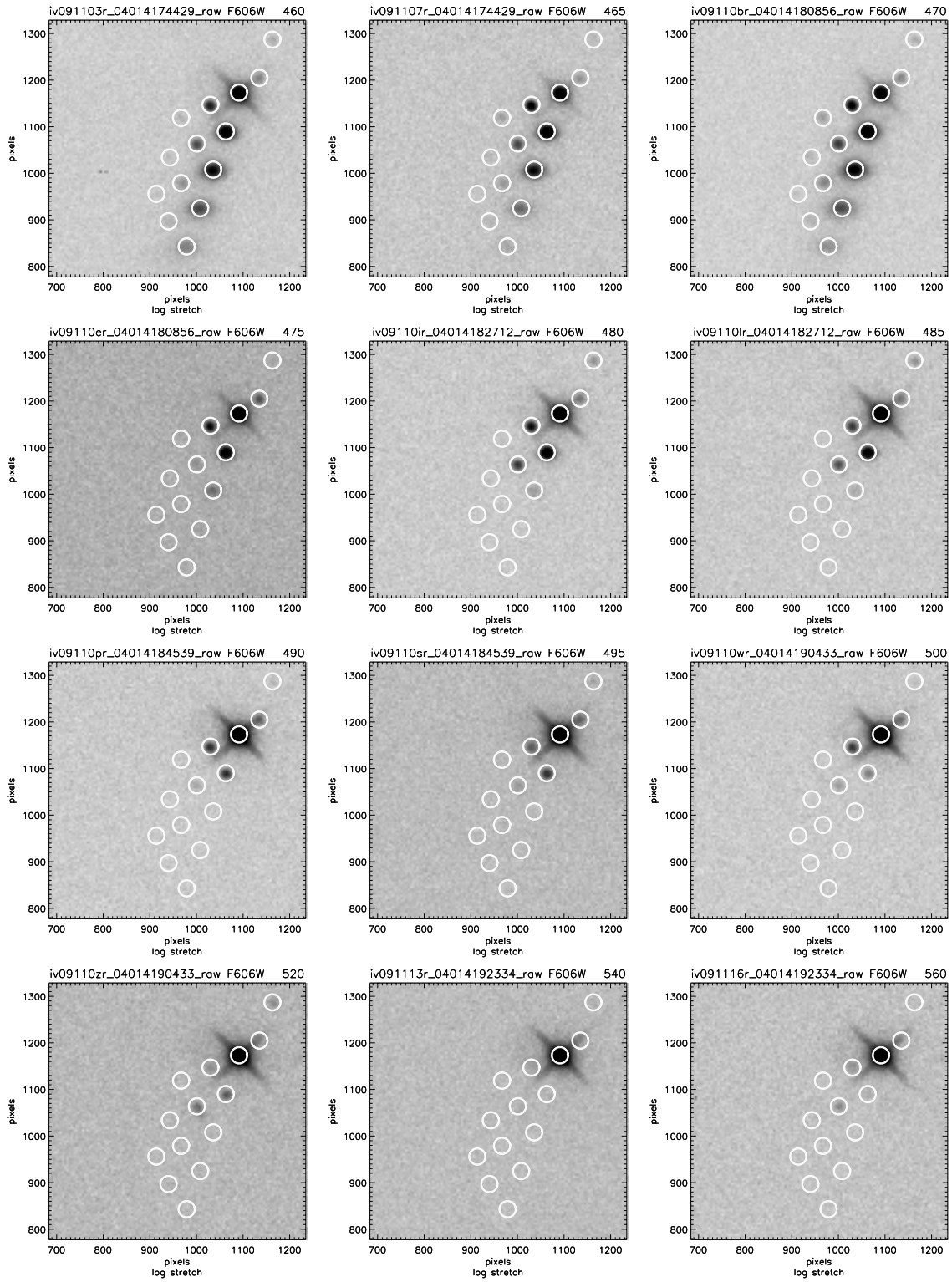

Figure 15 - Images of an extended source in monochromatic light with the F606W filter, from 460 to 730 nm (labeled), at a constant location on the detector. Each spot ghost has its own wavelength dependence. The positions of the source and the thirteen ghosts detected are circled, and form an unusual geometric pattern.

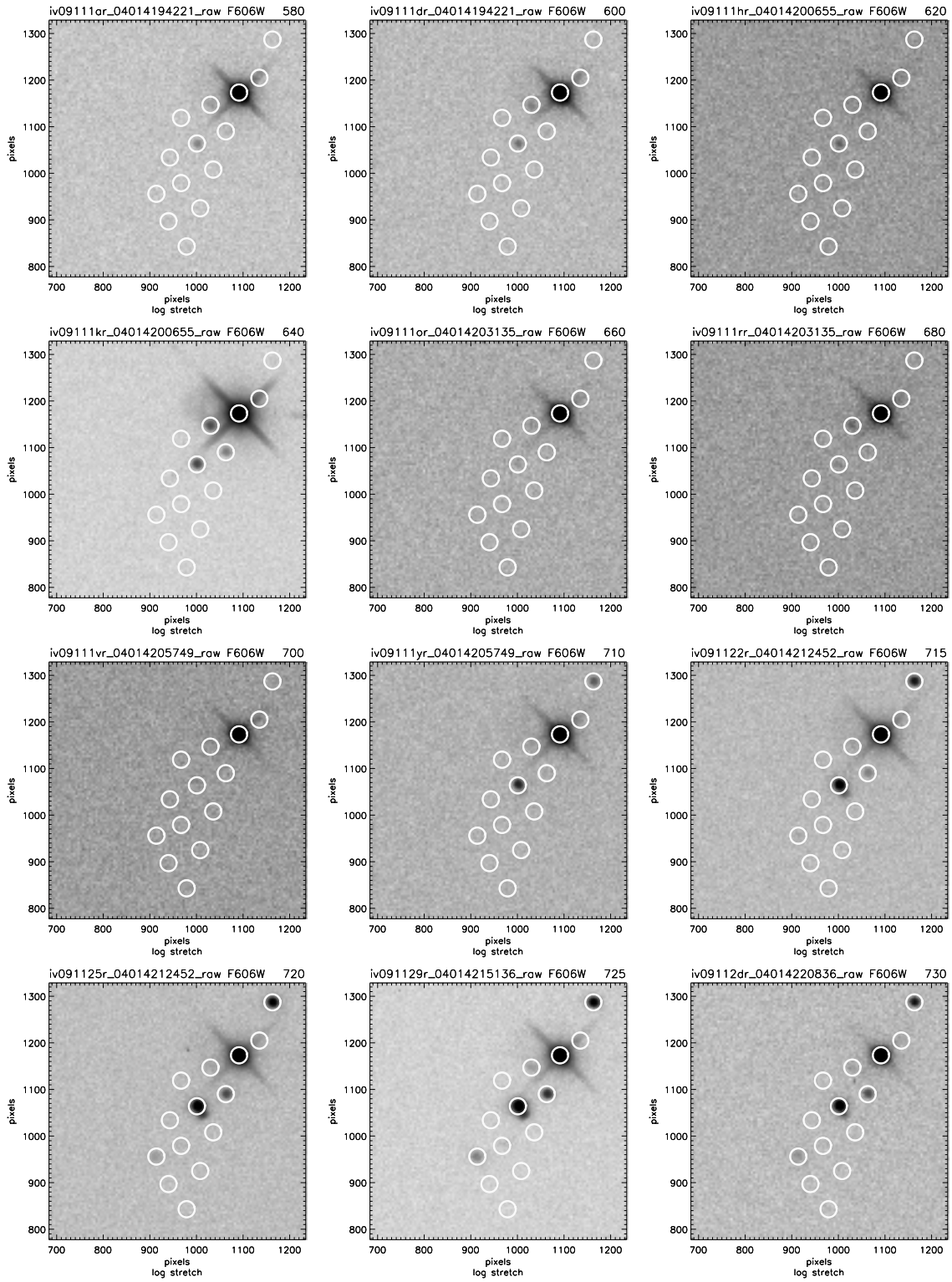

Figure 15 - continued.

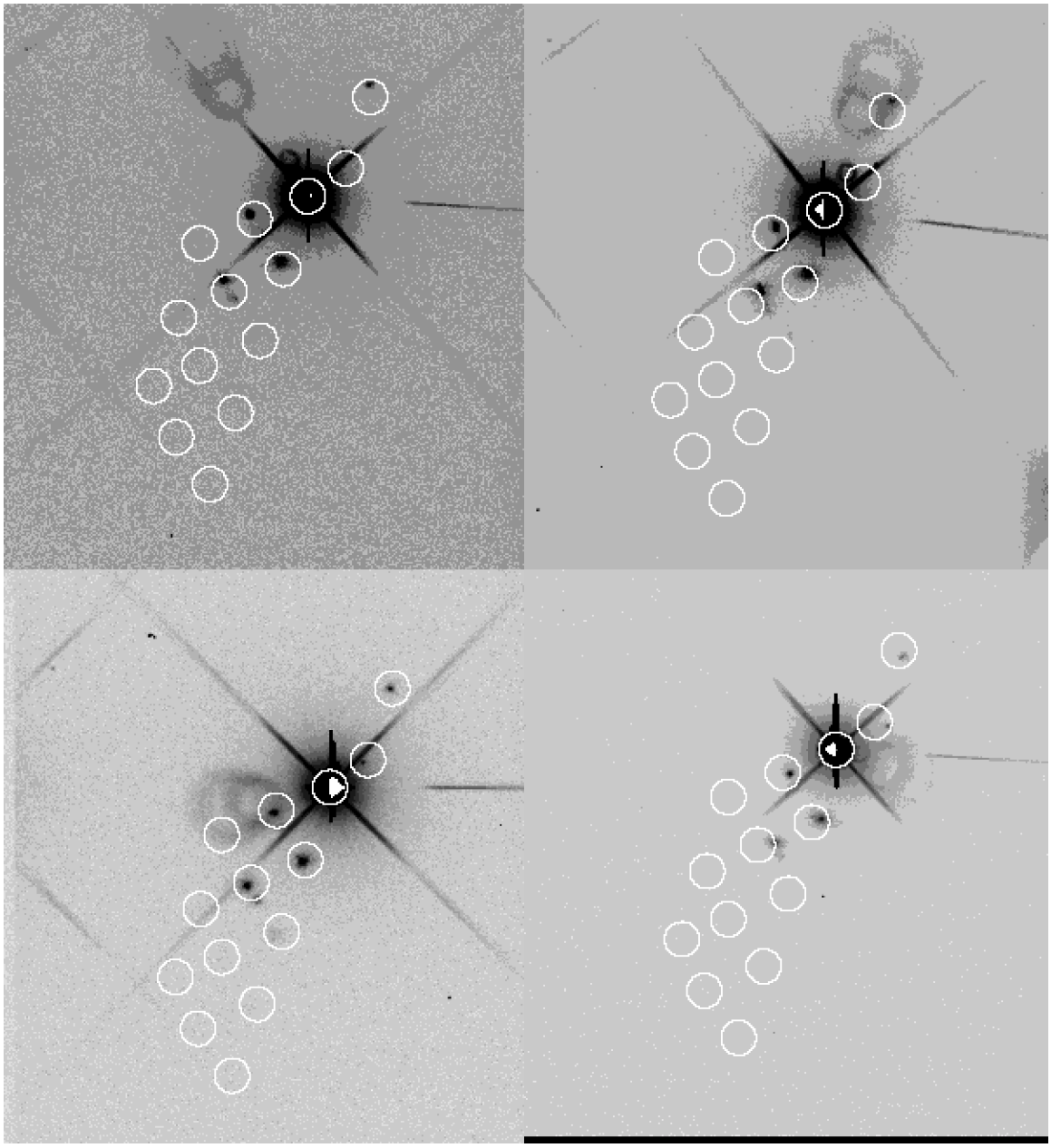

Figure 16 - Variation in the F606W spot ghosts with the position of the source in the field, again for each of the four detector quadrants. None of these positions on the detector is the same as that in **Figure 15**. However, the circles are plotted in the same location (relative to the source) as in **Figure 15**, demonstrating that the spot ghosts move slightly with respect to the primary image as a function of position on the detector. The horizontal feature to the right of the source is a test artifact. The spot ghosts are due to multiple reflections within a substrate, where the reflected beams travel a much shorter pathlength than reflections between layers (such as those reflections producing the larger filter ghosts of the air gap filters); the short pathlength is why these spot ghosts move (with respect to the primary image) very little as the source is moved around the detector.

Table 4: Strength of F606W Spot Ghosts vs. Wavelength*

wavelength (nm)	x,y 72,114	x,y 44,32	x,y -61,-26	x,y -124,-54	x,y -28,-83	x,y -90,-109	x,y -148,-139	x,y -55,-165	x,y -124,-194	x,y -177,-217	x,y -83,-248	x,y -151,-276	x,y -112,-330
460	6.9E-4	1.0E-3	9.9E-3	9.1E-4	7.6E-2	4.3E-3	6.2E-4	1.9E-2	1.3E-3	6.6E-4	5.6E-3	3.5E-4	1.6E-3
465	7.9E-4	3.2E-3	3.4E-2	1.8E-3	**1.7E-1**	9.2E-3	5.1E-4	3.0E-2	1.9E-3	8.7E-5	6.5E-3	9.0E-4	1.1E-3
470	1.1E-3	2.0E-3	3.7E-2	1.4E-3	**2.4E-1**	1.3E-2	1.4E-3	4.8E-2	4.0E-3	4.8E-4	9.9E-3	4.8E-4	1.4E-3
475	5.1E-5	3.9E-3	9.9E-3	1.6E-4	3.7E-2	6.4E-4	1.6E-4	3.5E-3	8.5E-3	1.6E-4	3.8E-4	1.7E-3	2.6E-5
480	7.7E-4	1.5E-3	8.1E-3	1.1E-4	3.2E-2	4.4E-3	1.1E-4	1.1E-3	3.9E-5	8.0E-5	9.0E-5	1.1E-4	8.0E-5
485	5.5E-4	7.3E-4	3.1E-3	6.2E-5	2.0E-2	2.3E-3	8.2E-5	4.8E-4	6.4E-5	9.8E-6	4.9E-5	6.2E-5	6.8E-5
490	7.8E-5	1.1E-3	2.9E-3	2.8E-5	2.6E-3	2.1E-4	5.5E-5	5.5E-5	2.7E-5	5.5E-5	1.1E-5	2.2E-5	4.4E-5
495	6.4E-4	6.4E-4	1.1E-3	5.6E-5	3.1E-3	1.7E-4	3.9E-4	5.2E-5	4.0E-4	3.6E-4	3.5E-4	2.3E-4	2.1E-4
500	2.8E-5	5.3E-4	2.3E-3	5.5E-5	7.1E-4	4.0E-4	2.8E-5	5.5E-5	5.5E-5	5.5E-5	3.2E-4	5.5E-5	1.1E-4
520	8.2E-4	7.0E-4	5.3E-4	2.1E-4	1.2E-3	7.9E-4	2.3E-4	2.0E-4	2.6E-4	7.5E-5	2.1E-4	2.6E-4	2.3E-4
540	1.4E-4	1.0E-3	6.1E-5	5.6E-4	7.5E-5	4.6E-5	3.8E-4	3.9E-4	3.4E-4	4.3E-4	3.7E-4	4.4E-4	2.5E-4
560	2.2E-5	8.2E-4	1.6E-4	3.9E-5	1.6E-4	6.1E-4	1.1E-4	2.4E-5	3.3E-6	5.9E-5	2.5E-5	6.9E-5	6.9E-5
580	4.5E-5	7.5E-4	5.3E-4	6.2E-4	5.7E-5	6.6E-4	7.1E-4	1.6E-5	8.4E-4	7.8E-5	6.6E-4	8.5E-4	7.8E-5
600	1.3E-4	6.4E-4	5.5E-4	3.8E-5	5.7E-5	1.1E-3	9.4E-5	9.4E-5	8.3E-5	1.0E-4	9.4E-5	9.4E-5	9.4E-5
620	1.9E-3	2.5E-4	1.9E-4	1.1E-3	1.2E-3	3.1E-3	8.0E-4	8.5E-4	1.0E-3	1.4E-3	8.9E-4	9.9E-4	1.4E-3
640	3.8E-5	7.6E-4	1.1E-3	3.0E-5	4.0E-4	1.6E-3	8.1E-5	4.3E-6	2.8E-5	1.8E-5	9.0E-6	1.1E-5	2.9E-5
660	1.5E-4	3.8E-4	4.2E-5	1.3E-4	6.2E-4	3.2E-4	2.7E-4	7.3E-5	1.9E-4	4.0E-4	9.8E-6	1.9E-4	1.9E-4
680	9.6E-4	1.8E-4	9.6E-4	6.8E-4	2.2E-4	1.5E-3	9.2E-4	1.2E-3	4.6E-4	5.8E-4	1.0E-3	8.0E-4	9.4E-4
700	1.1E-3	2.1E-4	2.8E-4	1.4E-3	2.8E-4	1.7E-3	9.1E-4	1.3E-3	5.3E-4	7.6E-4	6.7E-4	9.4E-4	1.3E-3
710	1.9E-3	1.3E-3	1.2E-4	4.6E-4	6.4E-4	5.1E-3	5.7E-4	3.5E-4	5.4E-4	5.3E-4	5.2E-4	2.9E-4	5.6E-4
715	7.2E-3	6.9E-4	9.7E-4	9.1E-5	1.0E-3	1.7E-2	6.9E-5	9.1E-5	3.4E-5	1.7E-4	1.6E-4	7.6E-4	2.8E-5
720	1.4E-2	5.4E-4	1.0E-3	3.0E-5	4.4E-3	2.9E-2	8.7E-5	3.1E-5	5.4E-5	6.7E-4	8.7E-5	5.7E-4	8.7E-5
725	1.4E-2	7.9E-4	1.0E-3	1.8E-5	6.2E-3	4.0E-2	3.7E-5	6.7E-5	4.7E-4	1.4E-3	5.4E-5	6.9E-5	2.7E-5
730	1.2E-2	2.0E-3	9.8E-4	2.5E-4	6.1E-3	3.9E-2	2.5E-4	2.5E-4	1.1E-4	2.4E-3	3.5E-5	2.9E-3	2.5E-4
735	4.7E-3	4.8E-4	2.6E-5	1.7E-4	2.2E-3	1.7E-2	2.0E-4	4.8E-4	4.8E-4	3.3E-4	4.8E-4	7.3E-5	1.6E-5

*Note that each spot ghost is identified by its x and y position relative to the source for the source location used during the monochromatic tests (**Figure 15**). The position of the spot ghosts relative to the source varies by a few pixels as the source is moved on the detector (**Figure 16**).

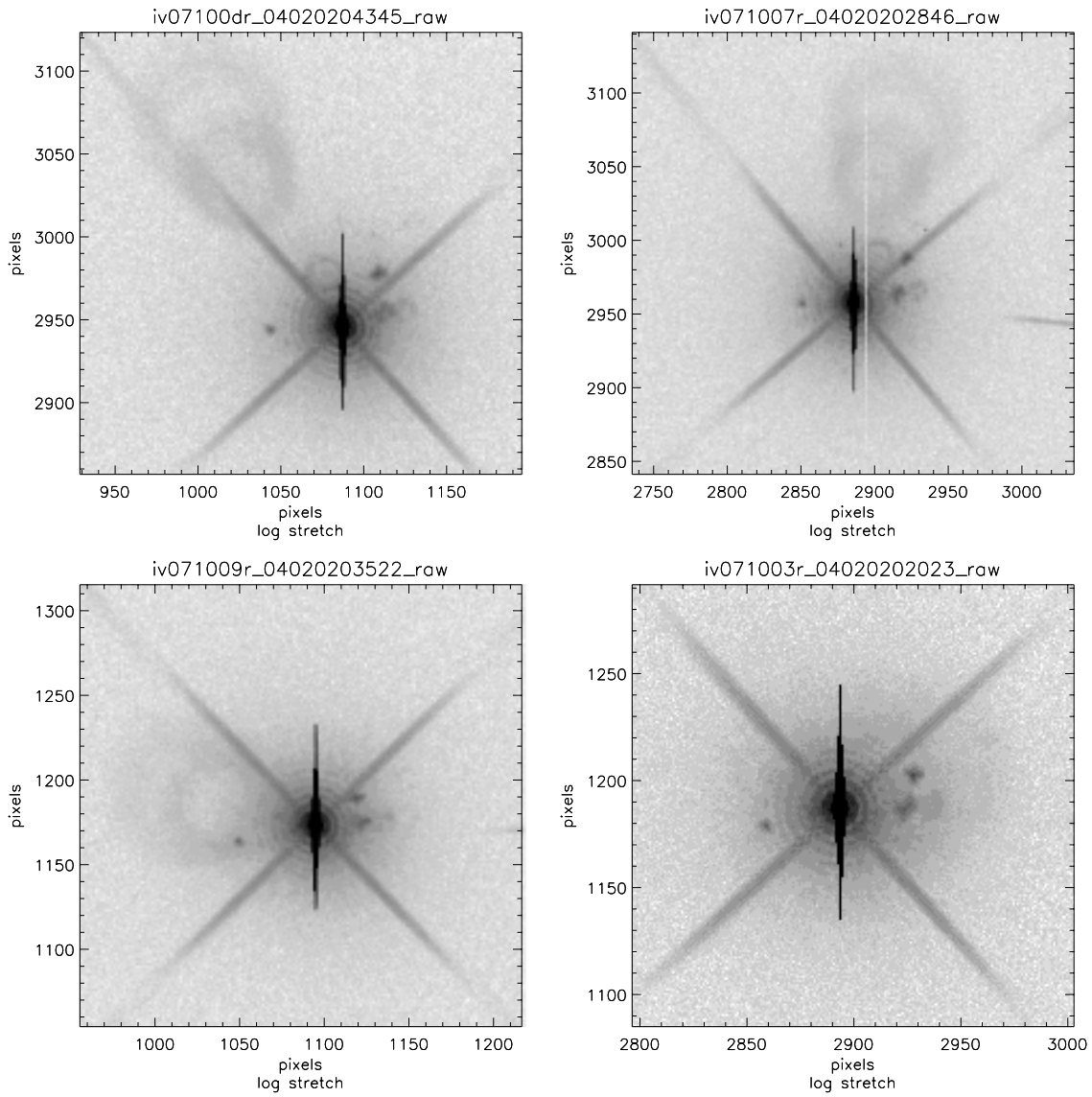

Figure 17 - F621M white light images (log stretch & saturated) with the source in each quadrant. The large black vertical feature is bleeding from the saturated source, the horizontal feature to the right of the source is a test artifact, and the large white vertical feature on the upper right is a dead detector column. Note that the window ghosts (large donuts) move significantly with respect to the source as the source is moved around the detector, but the compact filter ghosts move very little, as seen in the F606W (**Figures 14-16**). The flux in the two larger donuts is 0.3% of the source flux, while the flux in the smaller donuts (near the source) is 0.1% of the source flux. The flux in the brightest spot ghost is 0.1% of the source flux.

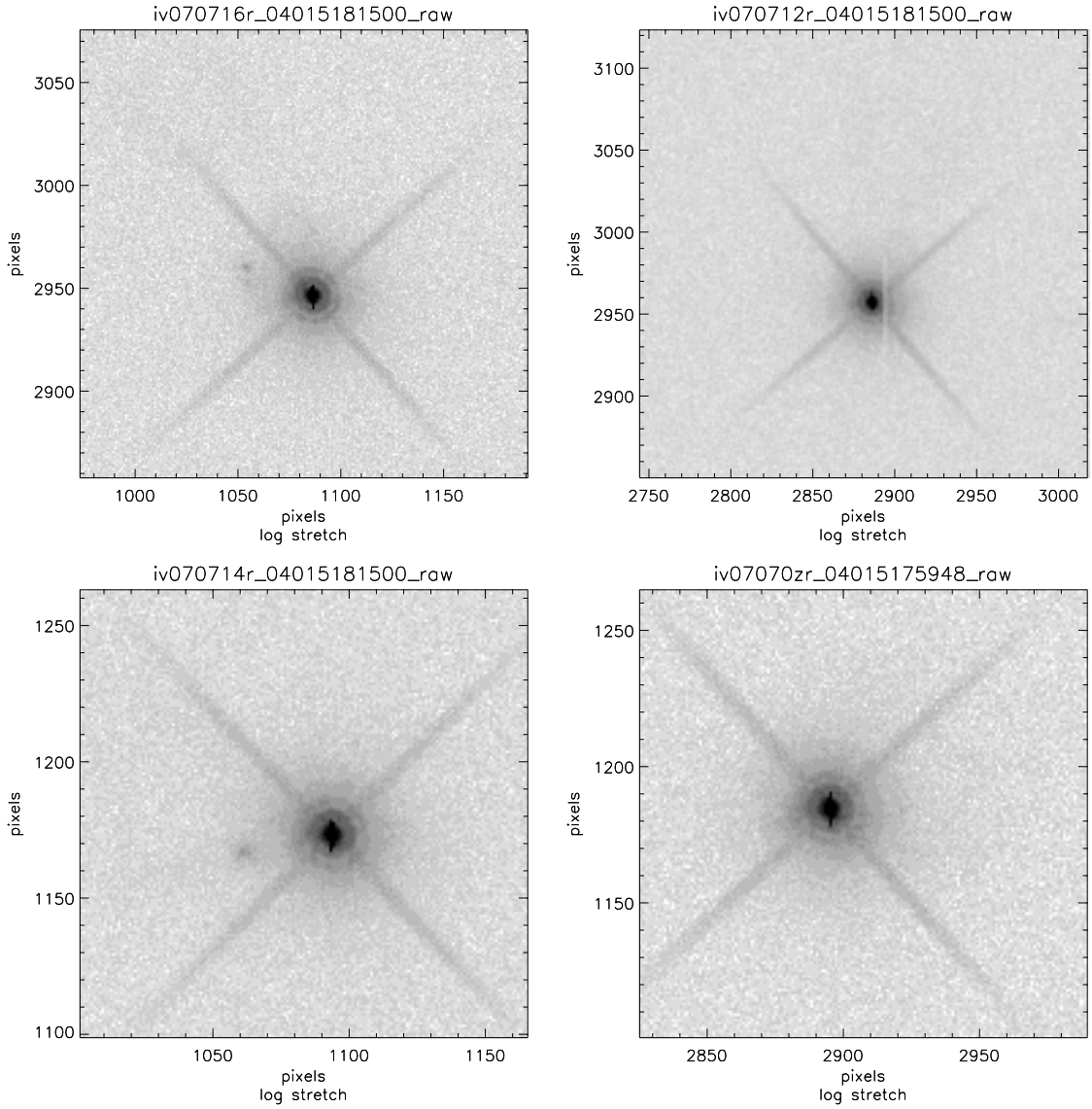

Figure 18 - F625W white light images (log stretch & saturated) with the source in each quadrant. The vertical feature on the upper right is a dead detector column. Very faint window ghosts and compact filter ghosts are present. The flux in the brightest spot ghost is 0.05% of the source flux.

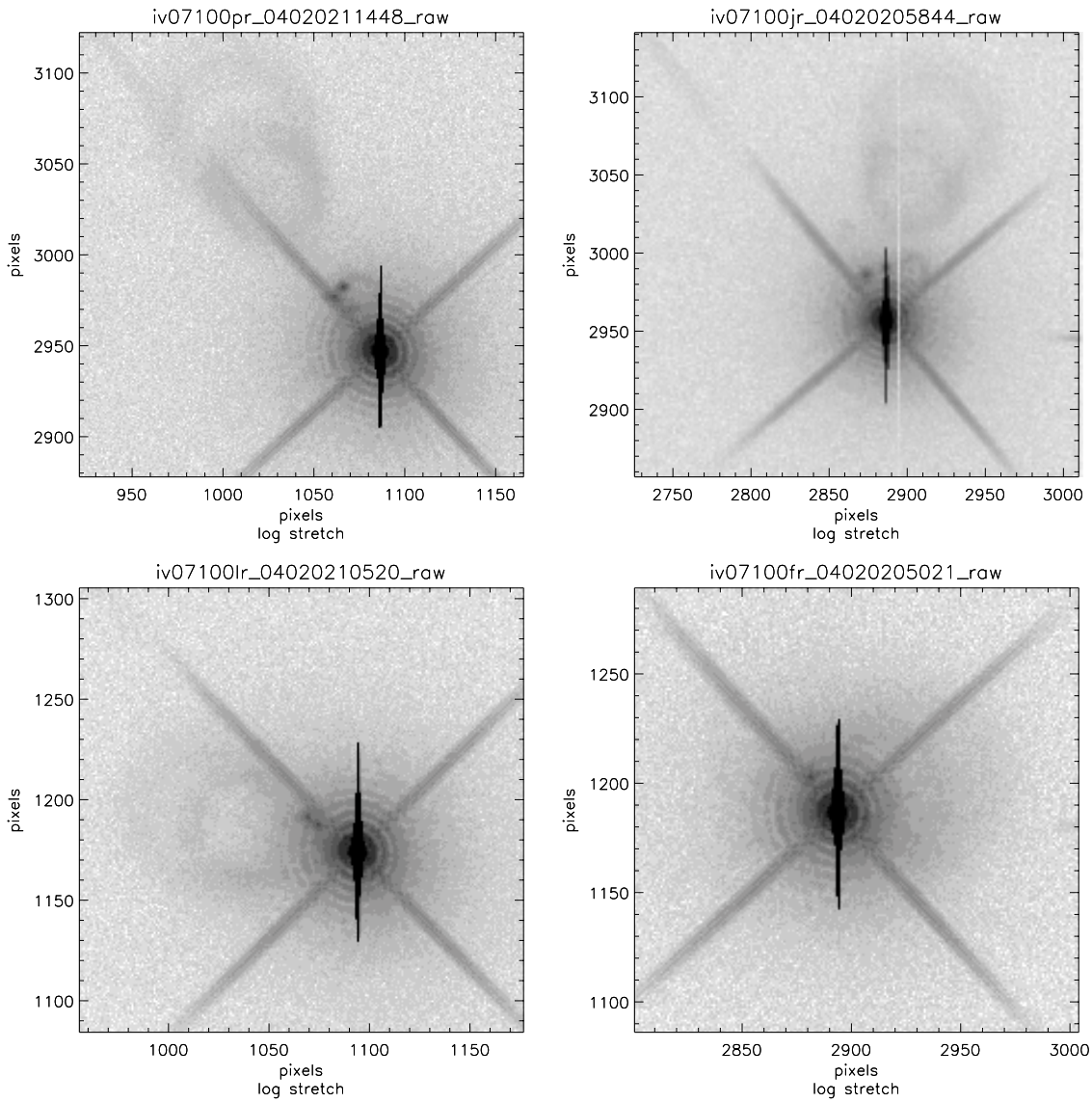

Figure 19 - F689M white light images (log stretch & saturated) with the source in each quadrant. The large black vertical feature is bleeding from the saturated source, the horizontal feature to the right of the source is a test artifact, and the large white vertical feature on the upper right is a dead detector column. Note again that the position of the window ghosts, relative to the source, changes significantly with source position on the detector, but the compact ghosts move very little, as in the F606W (**Figures 14-16**).The total flux in donuts is about 0.5% of the source flux, while the flux in the brightest spot ghost is 0.1% of the source flux.

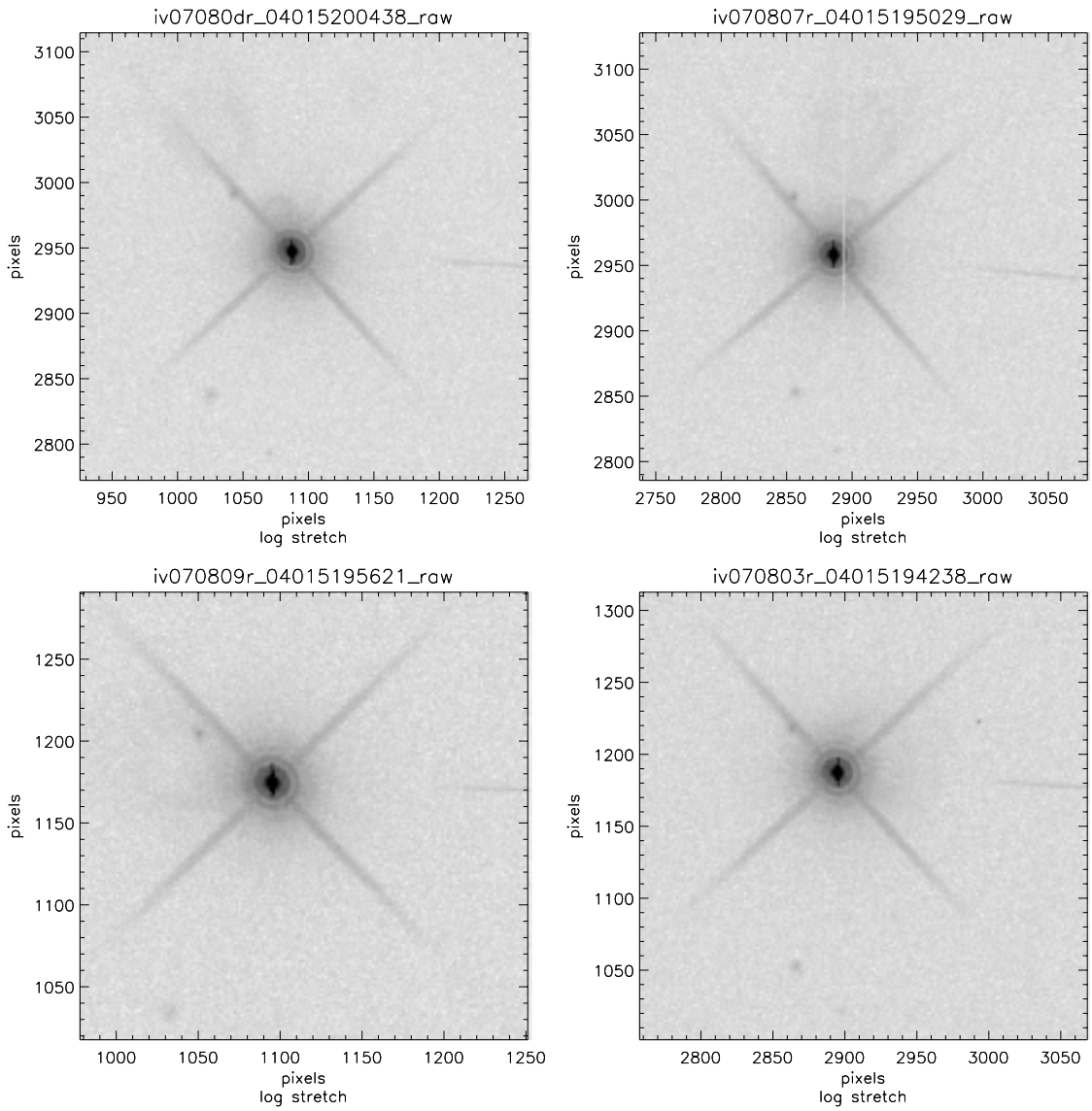

Figure 20 - F775W white light images (log stretch & saturated) with the source in each quadrant. The horizontal feature to the right of the source is a test artifact, and the vertical feature in the upper right quadrant is a dead detector column. As with the F606W, faint window ghosts can be seen moving significantly, relative to the source, but the compact filter ghosts do not move significantly, relative to the source. The flux in the brightest spot ghost is about 0.04% of the source flux.

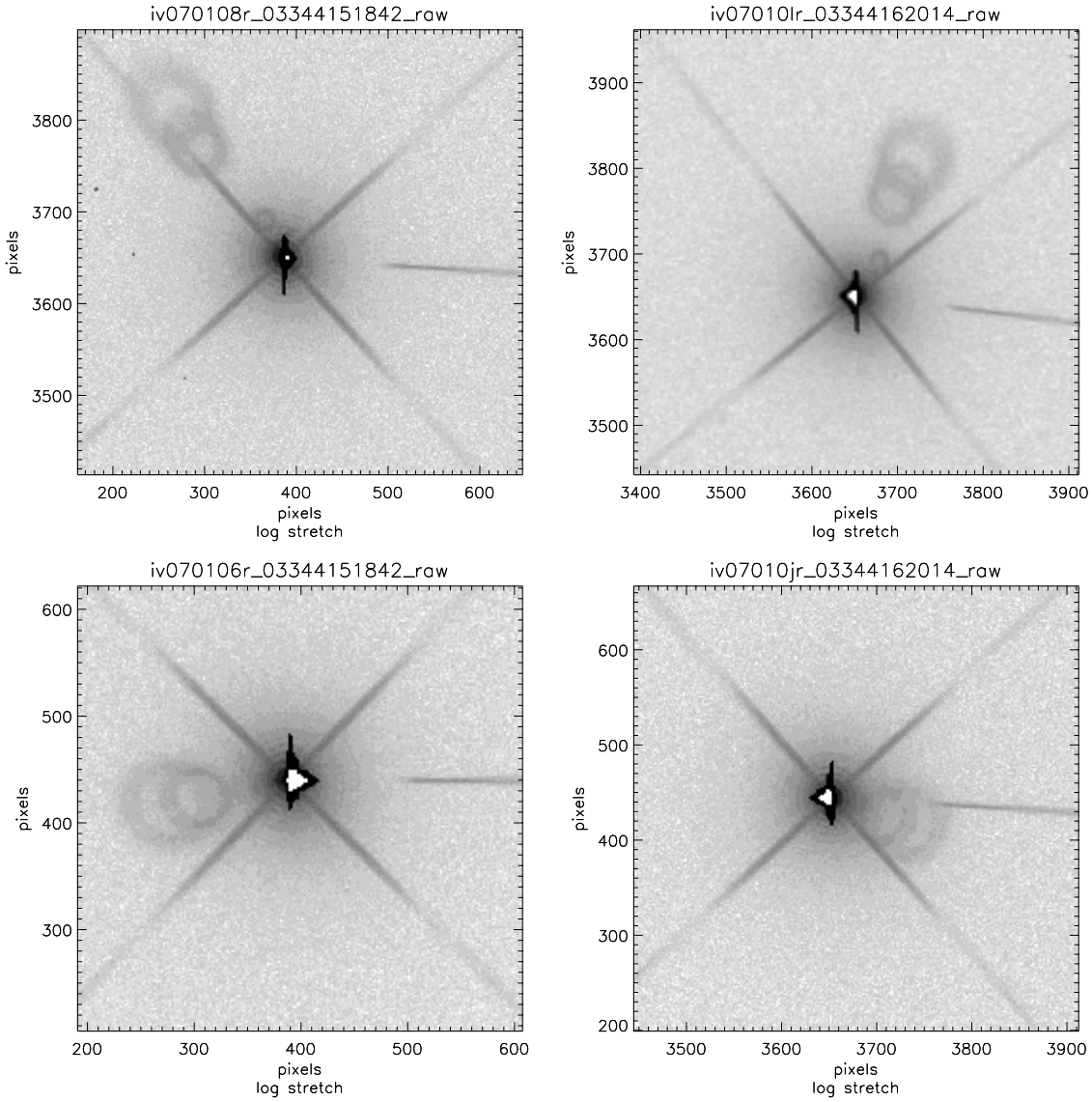

Figure 21 - F814W white light images (log stretch & saturated) with the source in each quadrant. The image was taken with 2x2 binning but the pixel coordinates shown here reflect distances in unbinned pixels. The horizontal feature to the right of the source is a test artifact. Three window ghosts (donuts) are present; the flux in the two interlocking donuts is about 0.4%, while the flux in the smaller donut is about 0.1%.

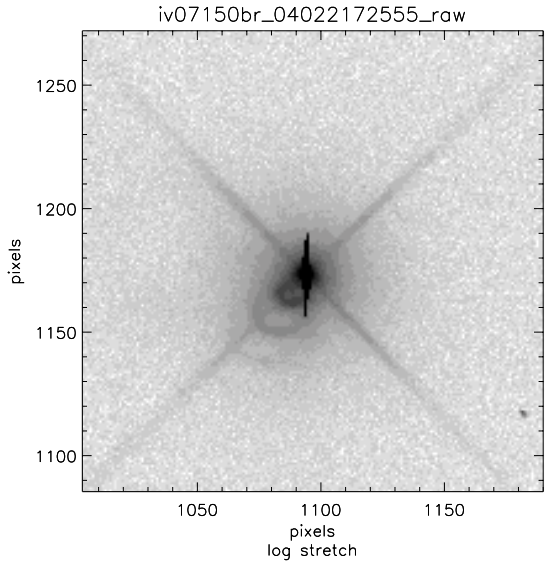

Figure 22 - FQ232N white light image (log stretch & saturated). This is a quad filter, so no field dependence is available for the ghosts (each detector quadrant has a different filter). This filter and FQ243N (**Figure 23**) are both on the same quad filter. Two interlocking filter ghosts can be seen (donuts); the flux in the brighter ghost is 4% of the source flux, while the flux in the fainter ghost is 1% of the source flux.

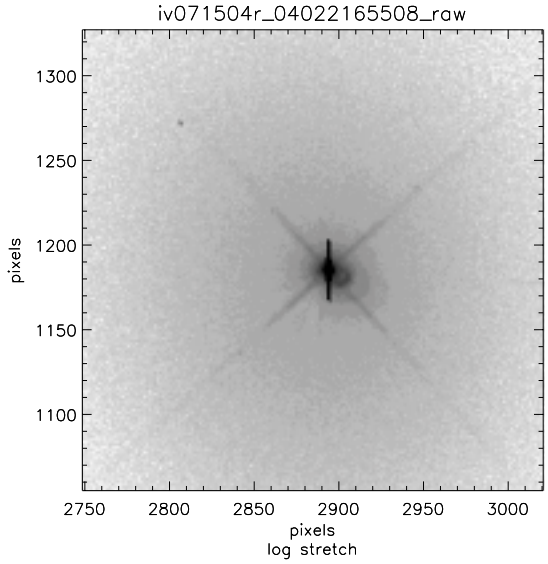

Figure 23 - FQ243N white light image (log stretch & saturated). This is a quad filter, so no field dependence is available for the ghosts (each detector quadrant has a different filter). Note the large halo around the primary image, which might indicate degradation of the filter surface. This filter and FQ232N (**Figure 22**) are both on the same quad filter. Two interlocking filter ghosts can be seen (donuts); the flux in the brighter ghost is 2% of the source flux, while the flux in the fainter ghost is 1% of the source flux.

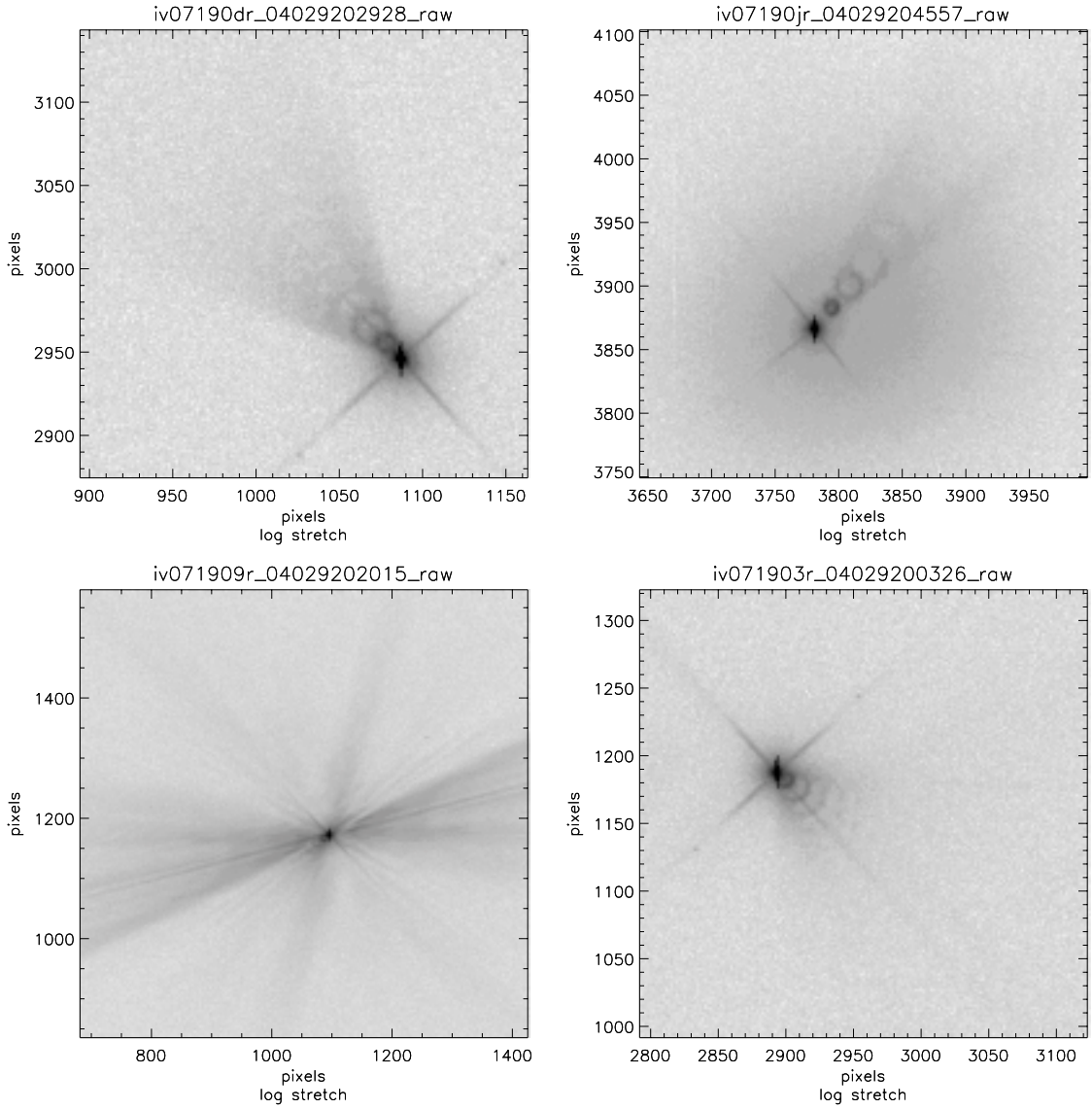

Figure 24 - F280N white light images (log stretch & saturated) with the source in each quadrant. Two of the quadrants show unusual images that are likely due to surface degradation: the source in the upper right quadrant has a large halo, while the source in the lower left quadrant shows strong scattered light. Images taken at other locations in the same quadrants (not shown) do not show these problems, so the degradation must be somewhat localized. On the other hand, a large fraction of the light is affected by the degradation, so the degradation must intercept a significant fraction of the beam as it passes through the filter. In the field points that do not show possible surface degradation, the flux in the chain of interlocking filter ghosts (donuts) is about 10% of the source flux.

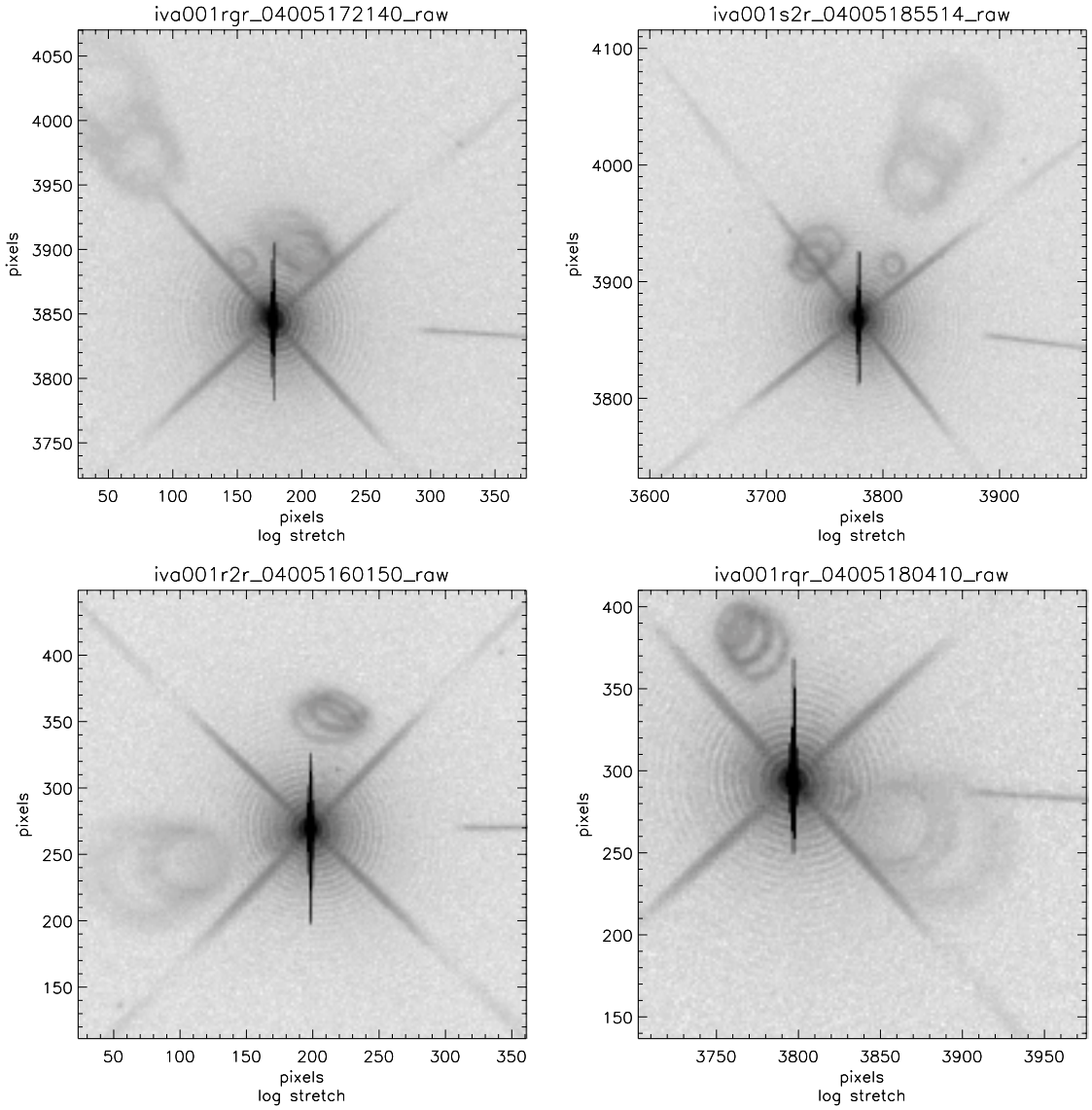

Figure 25 - F656N white light images (log stretch & saturated) with the source in each quadrant. This is an air gap filter. Donut-shaped window ghosts and donut-shaped filter ghosts are both present. The window ghosts are fainter and more extended than the filter ghosts. As the source is moved on the detector, the window ghost movement (relative to the source) is larger than that of the filter ghosts. The horizontal feature to the right of the source is a test artifact. The flux in the small window ghost, nearest the source, is about 0.1% of the source flux, while the flux in the larger interlocking window ghosts is 0.3% of the source flux. The flux in the interlocking filter ghosts is about 0.5% of the source flux.

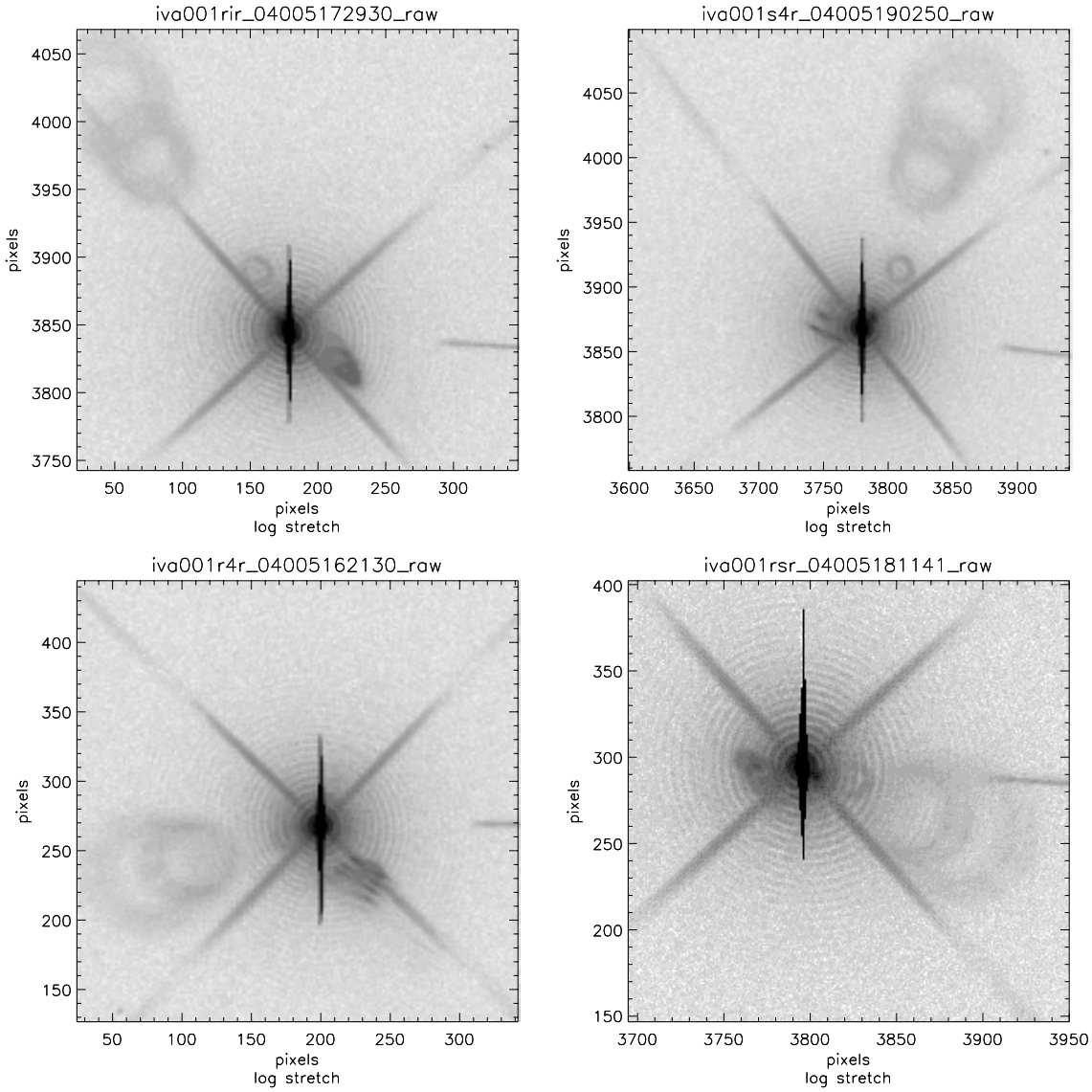

Figure 26 - F658N white light images (log stretch & saturated) with the source in each quadrant. This is an air gap filter. Donut-shaped window ghosts and donut-shaped filter ghosts are both present. The window ghosts are fainter and more extended than the filter ghosts. As the source is moved on the detector, the window ghost movement (relative to the source) is larger than that of the filter ghosts. The horizontal feature to the right of the source is a test artifact. The flux in the larger window ghosts (donuts) is about 0.4% of the source flux, while the flux in the filter ghost (compact) is about 0.9% of the source flux.

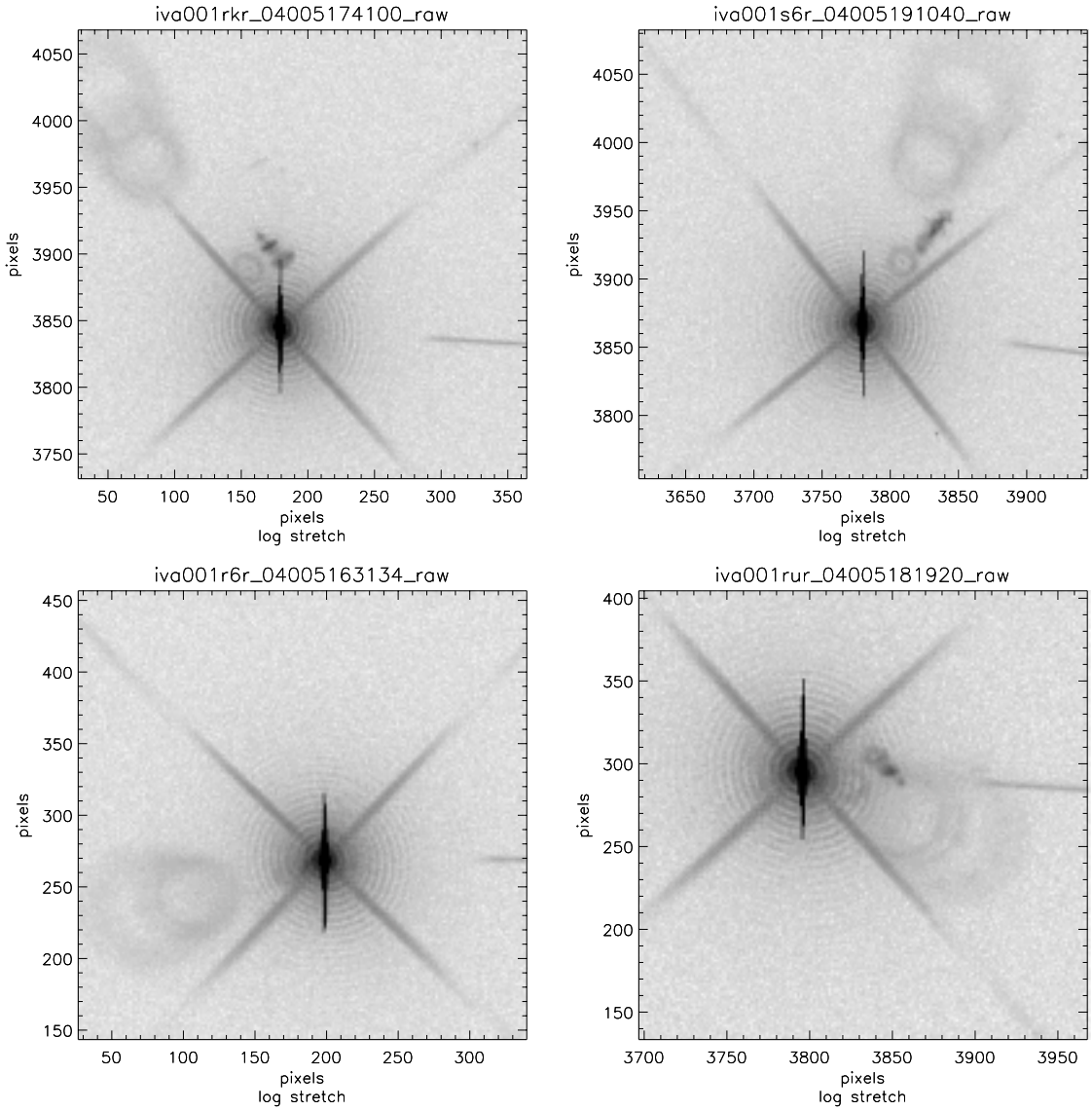

Figure 27 - F665N white light images (log stretch & saturated) with the source in each quadrant. This is an air gap filter. Donut-shaped window ghosts and donut-shaped filter ghosts are both present. The window ghosts are fainter and more extended than the filter ghosts. As the source is moved on the detector, the window ghost movement (relative to the source) is larger than that of the filter ghosts. The horizontal feature to the right of the source is a test artifact. The flux in the window donut ghosts is about 0.4% of the source flux, while the flux in the compact filter ghosts is about 0.4%.

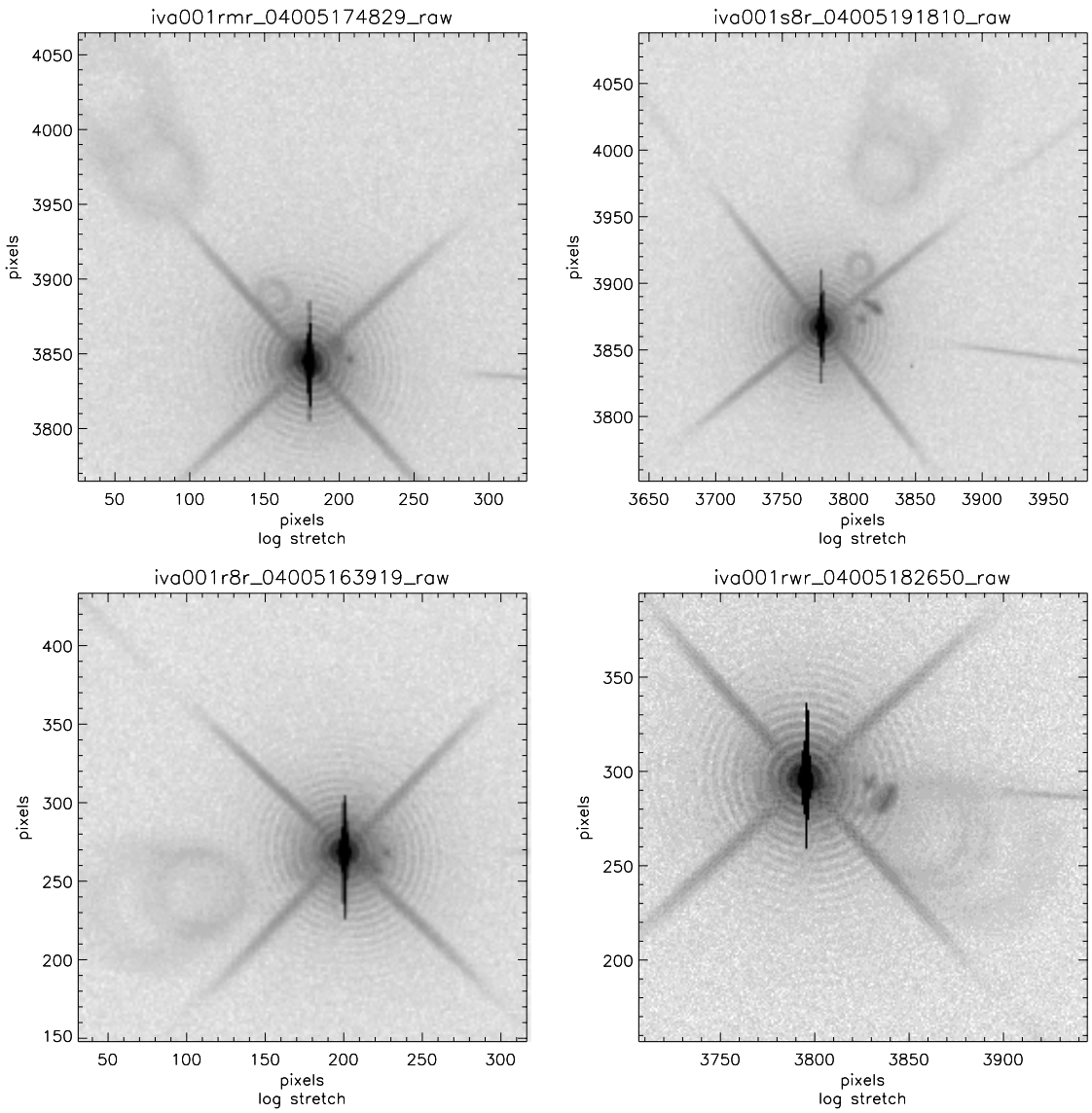

Figure 28 - F673N white light images (log stretch & saturated) with the source in each quadrant. This is an air gap filter. Donut-shaped window ghosts and donut-shaped filter ghosts are both present. The window ghosts are fainter and more extended than the filter ghosts. As the source is moved on the detector, the window ghost movement (relative to the source) is larger than that of the filter ghosts. The horizontal feature to the right of the source is a test artifact. The flux in the window donut ghosts is about 0.4% of the source flux, while the flux in the compact filter ghosts is about 0.3%.

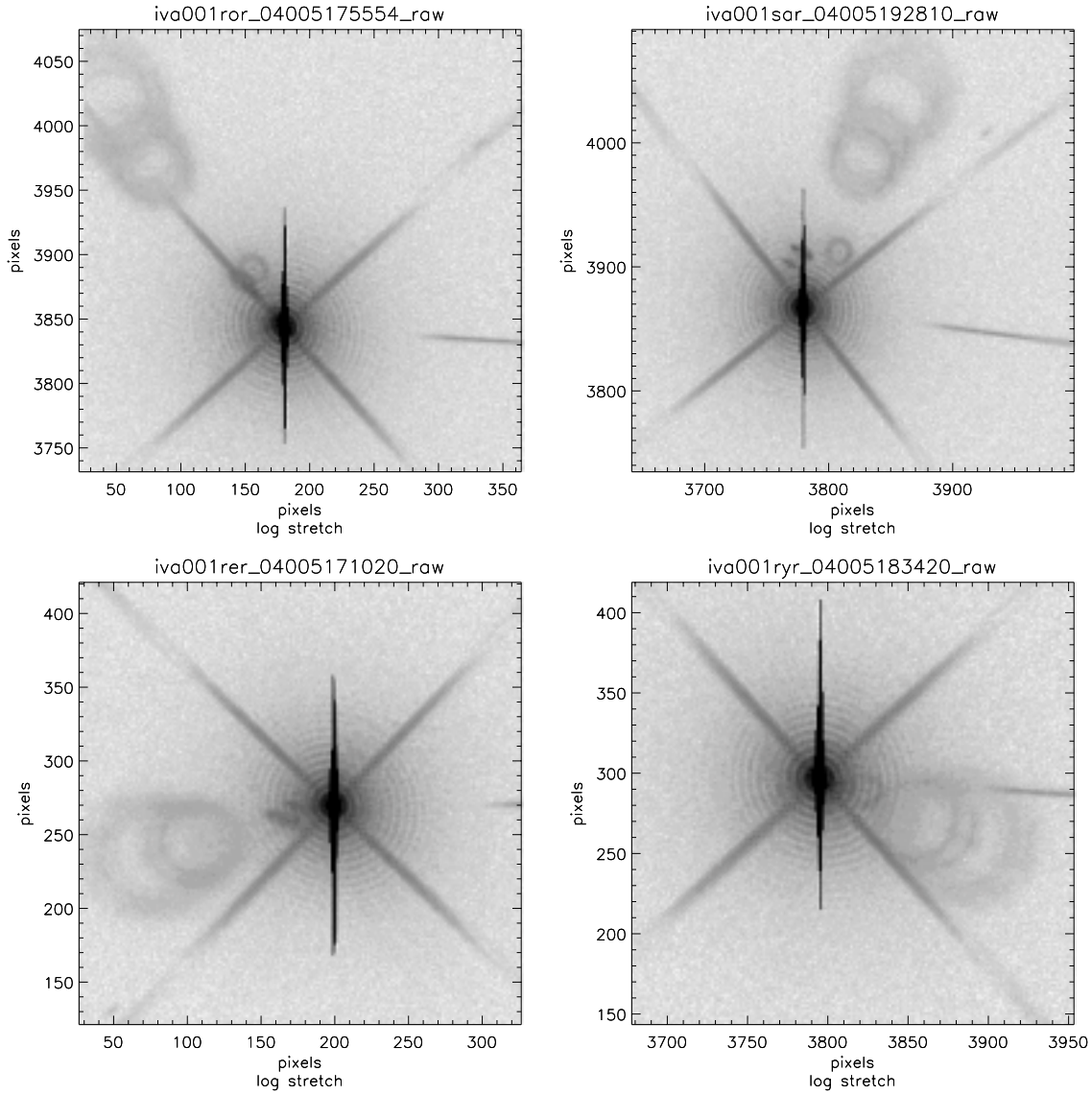

Figure 29 - F680N white light images (log stretch & saturated) with the source in each quadrant. This is an air gap filter. Donut-shaped window ghosts and donut-shaped filter ghosts are both present. The window ghosts are fainter and more extended than the filter ghosts. As the source is moved on the detector, the window ghost movement (relative to the source) is larger than that of the filter ghosts. The horizontal feature to the right of the source is a test artifact. The flux in the window donut ghosts is about 0.4% of the source flux, while the flux in the compact filter ghosts is about 0.3%.

Addressing the Filter Ghosts

The purpose of this report is to relate the results of the mini-calibration program, but given the ghosts that were found, it is worth noting briefly the work that is underway to address these problems. The descriptions here are preliminary, and the work will be explained more fully in a future report as the work progresses.

To review, there are two distinct categories of filter ghost. The first appears in the air gap filters, where the ghosts can be very strong (up to 15% of the primary image strength in white light); these ghosts vary strongly in position (relative to the source) and shape as the source is moved around the detector. The second type of filter ghost appears in the multiple-substrate filters that do not have an air gap; these ghosts are compact, have strengths less than 1% of the primary image in white light, and move little with respect to the source as the source is moved on the detector.

Engineers at GSFC are working to model both types of ghost, and have made significant progress in understanding the air gap ghosts. The models show that the ghosts likely originate in multiple reflections off the metal blocking layer, and qualitatively predict the shape, position, and wavelength dependence of these ghosts. These models underpredict the ghost strengths, but the ghost strength is a significant function of the filter transmission at wavelengths just beyond the nominal bandpass, where the transmission is changing rapidly; the models should improve as the filter transmission is characterized more accurately. The compact ghosts seen in the multiple-substrate filters (with no air gap) are caused by reflections within a substrate, but models of these ghosts are not yet as advanced as those for the extended filter ghosts found in the air gap filters.

In parallel to this modelling, the STScI WFC3 team and the engineers at GSFC are investigating 4 paths to mitigate the ghosts in the filters with the most serious problems:

- Replace the filters using a new design. Barr is prototyping new F218W, F225W, and F300X filters that do not have an air gap. Testing of transmission and ghost properties for the first of these prototypes is now underway.
- Replace the filters with the flight spares. Some of the filters have spares with similar transmission performance. We are now characterizing their ghost properties. Any filters with significantly better ghost properties could be swapped with the current flight filters.
- Introduce a wedge into the original air gap design. The existing filters cannot be disassembled, but new filters with the same design could be constructed with a large wedge to move the reflections off the detector. Preliminary models indicate a 4 degree wedge would be needed, while the filter wheel can only accommodate a wedge of 2.3 degrees, so this avenue is not promising.

- Separate the substrates for a filter onto two distinct filter wheels. By trading away a lower priority filter, one substrate in an air-gap filter can be moved to a different wheel, allowing the 4 degree wedge between substrates.

Scientific Impact

It is early to decide the scientific impact of the filter ghosts, because work is underway to mitigate them. Scientific impact will be explored more fully in a future report, when the status of the filters will be more mature. However, it is worth noting a few points if we were to fly with the current filter set.

- Most of the filters have no significant ghosting. Although we showed images from every filter with detectable ghosts in this report, it is important to keep in mind that the images were heavily saturated and plotted with a logarithmic stretch, for clarity. If one excludes the ghosts caused by reflections between the CCD and window (which only produce ghosts for sources in the extreme lower right hand corner), only a handful of filters show serious ghosts that are either numerous (e.g., F606W) or well above the acceptable strength (e.g., F218W and F225W).
- To avoid interpretation of ghosts as astrophysical objects or structure, a complete library of images should be obtained in every filter with significant ghosts, as a function of position on the detector and spectral type. This library would include ground images, theoretical ghost models, and flight images.
- For point source photometry, ghosts would be difficult to remove via point-spread-function (PSF) fitting, due to the unusual wavelength and position dependence of the ghosts. Most PSF-fitting software can handle PSFs with some field-dependence, but the variation in ghost position, shape, and strength is beyond the capabilities of codes available now (to the best of our knowledge). The additional wavelength dependence would complicate PSF-fitting enormously (e.g., the relative strengths of the compact ghosts in F606W would be a function of spectral type in a crowded field).
- Because the position angle of the donut ghosts changes significantly with source position on the detector, rotation of the field would not necessarily mitigate these ghosts. E.g., imagine a bright point source with faint extended structure imaged using F680N (**Figure 29**). If one images the source in the upper left hand quadrant, and the structure is at 10:00, rotating the source to the lower right hand quadrant will place the structure at 4:00, and the ghosts would cover much of the structure in both cases. Instead, dithering would be a better option.
- Because compact ghosts like those in the F606W move little with respect to the source as the source is moved around the detector, dithering the field would do little to mitigate them. Rotation of the field would be a better option, with the ghosts treated similarly to cosmic ray impacts.

- Even for the filters with the strongest ghosts, it is important to keep in mind that the "white light" tests were performed with a very red spectrum (**Figure 3**). Because most of the ghost power in F218W and F225W comes from wavelengths redder than the nominal bandpass, hot sources would produce far weaker ghosts than those produced by the xenon lamp. Spectral types from O5-A5 would produce ghosts of 2-3% in the F218W and F225W filters - much smaller than the 10-15% seen during the ground testing with the xenon lamp. However, a G5 star produces ghosts similar to that of the xenon lamp, and cooler stars produce even stronger ghosts. In some astrophysical situations, this would not be a large problem. E.g., in a globular cluster, stars near the tip of the red giant branch (RGB) are 100 times more luminous than the hot horizontal branch (HB) stars, but in the F225W or F218W filters these same RGB stars would appear 100 times fainter than the hot HB stars, with their ghosts fainter still. On the other hand, if one were trying to detect ultraviolet emission associated with very cool stars, the ghosts could present a major problem. The bottom line is that the scientific impact should be explored more fully when the filter situation is resolved, using detailed simulations of various astrophysical situations.

Summary

The WFC3 mini-calibration demonstrated that most of the instrument is working very well. However, because of the increased blue sensitivity of the WFC3 and its detector optimization, we throroughly inspected the imaging quality of the instrument through its full suite of UVIS filters, and found significant ghosting in some cases. Several unexpected problems were found. First, the air gap filters show large, extended, donut ghosts, which can be very strong when imaging red sources with filters at the shortest wavelengths available on WFC3. Second, other filters without an air gap but with multiple substrates (e.g., F606W) show numerous faint ghosts that are very compact. Finally, two of the narrowband filters (F280N and F243N) show signs of surface degradation. Although most of the filters are performing well, we are investigating avenues for rectifying the ghost problems in the handful of filters with serious ghosting. These activities will be explained more fully in future reports.

Acknowledgements

We are grateful to the entire WFC3 teams at STScI and GSFC for their efforts in the mini-calibration and their assistance with the analysis and interpretation of these data.